Publication Year	2018
Acceptance in OA	2021-02-10T14:10:55Z
Title	Exploring cosmic origins with CORE: Gravitational lensing of the CMB
Authors	Challinor, A., Allison, R., Carron, J., Errard, J., Feeney, S., Kitching, T., Lesgourgues, J., Lewis, A., Zubeldía, Í., Achucarro, A., Ade, P., Tartari, A., Tomasi, M., Tramonte, D., Trappe, N., Trombetti, T., Tucker, C., Valiviita, J., Van de Weijgaert, R., van Tent, B., Vennin, V., Ashdown, M., Vielva, P., Vittorio, N., Young, K., Zannoni, M., Ballardini, M., Banday, A. J., Banerji, R., Bartlett, J., Bartolo, N., Basak, S., Baumann, D., Bersanelli, M., Bonaldi, A., BONATO, MATTEO, Borrill, J., Bouchet, F., Boulanger, F., Brinckmann, T., Bucher, M., BURIGANA, CARLO, Buzzelli, A., Cai, Z. -Y., Calvo, M., Carvalho, C. -S., Castellano, G., Chluba, J., Clesse, S., Colantoni, I., Coppolecchia, A., Crook, M., d'Alessandro, G., de Bernardis, P., de Gasperis, G., De Zotti, G., Delabrouille, J., Di Valentino, E., Diego, J. -M., Fernandez-Cobos, R., Ferraro, S., FINELLI, FABIO, Forastieri, F., Galli, S., Genova-Santos, R., Gerbino, M., González-Nuevo, J., Grandis, S., Greenslade, J., Hagstotz, S., Hanany, S., Handley, W., Hernandez-Monteagudo, C., Hervías-Caimapo, C., Hills, M., Hivon, E., Kiiveri, K., Kisner, T., Kunz, M., Kurki-Suonio, H., Lamagna, L., Lasenby, A., Lattanzi, M., Liguori, M., Lindholm, V., López-Caniego, M., Luzzi, G., Maffei, B., Martinez-González, E., Martins, C. J. A. P., Masi, S., Matarrese, S., McCarthy, D., Melchiorri, A., Melin, J. -B., Molinari, D., Monfardini, A., Natoli, P., Negrello, M., Notari, A., Paiella, A., PAOLETTI, DANIELA, Patanchon, G., Piat, M., Pisano, G., Polastri, L., Polenta, G., Pollo, A., Poulin, V., Quartin, M., Remazeilles, M., Roman, M., Rubino-Martin, J. -A., Salvati, L.
Publisher's version (DOI)	10.1088/1475-7516/2018/04/018
Handle	http://hdl.handle.net/20.500.12386/30287
Journal	JOURNAL OF COSMOLOGY AND ASTROPARTICLE PHYSICS
Volume	2018

Prepared for submission to JCAP

Exploring cosmic origins with CORE: gravitational lensing of the CMB

Anthony Challinor,[1,2,3] **Rupert Allison,**[1,2] **Julien Carron,**[4] **Josquin Errard,**[5] **Stephen Feeney,**[6] **Thomas Kitching,**[7] **Julien Lesgourgues,**[8] **Antony Lewis,**[4] **Íñigo Zubeldía,**[1,2] **Ana Achucarro,**[9,10] **Peter Ade,**[11] **Mark Ashdown,**[12,2] **Mario Ballardini,**[13,14,15] **A. J. Banday,**[16,17] **Ranajoy Banerji,**[18] **James Bartlett,**[18] **Nicola Bartolo,**[19,20,21] **Soumen Basak,**[22,23] **Daniel Baumann,**[24] **Marco Bersanelli,**[25,26] **Anna Bonaldi,**[27] **Matteo Bonato,**[28,29] **Julian Borrill,**[30] **François Bouchet,**[31] **François Boulanger,**[32] **Thejs Brinckmann,**[8] **Martin Bucher,**[18] **Carlo Burigana,**[14,15,33] **Alessandro Buzzelli,**[34,35,36] **Zhen-Yi Cai,**[37] **Martino Calvo,**[38] **Carla-Sofia Carvalho,**[39] **Gabriella Castellano,**[40] **Jens Chluba,**[27] **Sebastien Clesse,**[8] **Ivan Colantoni,**[40] **Alessandro Coppolecchia,**[34,41] **Martin Crook,**[42] **Giuseppe d'Alessandro,**[34,41] **Paolo de Bernardis,**[34,41] **Giancarlo de Gasperis,**[34,36] **Gianfranco De Zotti,**[21] **Jacques Delabrouille,**[18] **Eleonora Di Valentino,**[31,43] **Jose-Maria Diego,**[10] **Raul Fernandez-Cobos,**[44] **Simone Ferraro,**[45] **Fabio Finelli,**[14,15] **Francesco Forastieri,**[46] **Silvia Galli,**[31] **Ricardo Genova-Santos,**[47,48] **Martina Gerbino,**[49,50] **Joaquin González-Nuevo,**[51] **Sebastian Grandis,**[52,53] **Joshua Greenslade,**[54] **Steffen Hagstotz,**[52,53] **Shaul Hanany,**[55] **Will Handley,**[12,2] **Carlos Hernandez-Monteagudo,**[56] **Carlos Hervías-Caimapo,**[27] **Matthew Hills,**[42] **Eric Hivon,**[31] **Kimmo Kiiveri,**[57,58] **Ted Kisner,**[30] **Martin Kunz,**[59] **Hannu Kurki-Suonio,**[57,58] **Luca Lamagna,**[34,41] **Anthony Lasenby,**[12,2] **Massimiliano Lattanzi,**[46] **Michele Liguori,**[13,20,21] **Valtteri Lindholm,**[57,58] **Marcos López-Caniego,**[60] **Gemma Luzzi,**[34] **Bruno Maffei,**[32] **Enrique Martinez-González,**[44] **C.J.A.P. Martins,**[61] **Silvia Masi,**[34,41] **Darragh McCarthy,**[62] **Alessandro Melchiorri,**[34,41] **Jean-Baptiste Melin,**[63] **Diego Molinari,**[33,46,14] **Alessandro Monfardini,**[38] **Paolo Natoli,**[33,46] **Mattia Negrello,**[11] **Alessio Notari,**[64] **Alessandro Paiella,**[34,41] **Daniela Paoletti,**[14] **Guillaume Patanchon,**[18] **Michel Piat,**[18] **Giampaolo Pisano,**[11] **Linda Polastri,**[33,45] **Gianluca Polenta,**[65,66] **Agnieszka Pollo,**[67] **Vivian Poulin,**[8,68] **Miguel**

Quartin,[69,70] Mathieu Remazeilles,[27] Matthieu Roman,[71] Jose-Alberto Rubino-Martin,[47,48] Laura Salvati,[34,41] Andrea Tartari,[18] Maurizio Tomasi,[25] Denis Tramonte,[47] Neil Trappe,[62] Tiziana Trombetti,[14] Carole Tucker,[11] Jussi Valiviita,[57,58] Rien Van de Weijgaert,[72,73] Bartjan van Tent,[74] Vincent Vennin,[75] Patricio Vielva,[44] Nicola Vittorio,[34,36] Karl Young,[54] and Mario Zannoni,[76,77] for the CORE collaboration.

[1]Institute of Astronomy, Madingley Road, Cambridge CB3 0HA, UK

[2]Kavli Institute for Cosmology Cambridge, Madingley Road, Cambridge CB3 0HA, UK

[3]DAMTP, Centre for Mathematical Sciences, Wilberforce Road, Cambridge CB3 0WA, UK

[4]Department of Physics and Astronomy, University of Sussex, Falmer, Brighton BN1 9QH, UK

[5]Institut Lagrange, LPNHE, Place Jussieu 4, 75005 Paris, France

[6]Center for Computational Astrophysics, 160 5th Avenue, New York, NY 10010, USA

[7]Mullard Space Science Laboratory, University College London, Holmbury St Mary, Dorking, Surrey RH5 6NT, UK

[8]Institute for Theoretical Particle Physics and Cosmology (TTK), RWTH Aachen University, D-52056 Aachen, Germany.

[9]Instituut-Lorentz for Theoretical Physics, Universiteit Leiden, 2333 CA, Leiden, The Netherlands

[10]Department of Theoretical Physics, University of the Basque Country UPV/EHU, 48040 Bilbao, Spain

[11]School of Physics and Astronomy, Cardiff University, The Parade, Cardiff CF24 3AA, UK

[12]Astrophysics Group, Cavendish Laboratory, Cambridge, CB3 0HE, UK

[13]DIFA, Dipartimento di Fisica e Astronomia, Universitá di Bologna, Viale Berti Pichat, 6/2, I-40127 Bologna, Italy

[14]INAF/IASF Bologna, via Gobetti 101, I-40129 Bologna, Italy

[15]INFN, Sezione di Bologna, Via Irnerio 46, I-40127 Bologna, Italy

[16]Université de Toulouse, UPS-OMP, IRAP, F-31028 Toulouse cedex 4, France

[17]CNRS, IRAP, 9 Av. colonel Roche, BP 44346, F-31028 Toulouse cedex 4, France

[18]APC, AstroParticule et Cosmologie, Université Paris Diderot, CNRS/IN2P3, CEA/Irfu, Observatoire de Paris Sorbonne Paris Cité, 10, rue Alice Domon et Leonie Duquet, 75205 Paris Cedex 13, France

[19]Dipartimento di Fisica e Astronomia "Galileo Galilei", Università degli Studi di Padova, Via Marzolo 8, I-35131, Padova, Italy

[20]INFN, Sezione di Padova, Via Marzolo 8, I-35131 Padova, Italy

[21]INAF-Osservatorio Astronomico di Padova, Vicolo dell'Osservatorio 5, I-35122 Padova, Italy

[22]Department of Physics, Amrita School of Arts & Sciences, Amritapuri, Amrita Vishwa Vidyapeetham, Amrita University, Kerala 690525, India

[23]SISSA, Via Bonomea 265, 34136, Trieste, Italy

[24]Institute of Physics, University of Amsterdam, Amsterdam, 1090 GL, The Netherlands

[25]Dipartimento di Fisica, Università degli Studi di Milano, Via Celoria 16, I-20133 Milano, Italy
[26]INAF IASF, Via Bassini 15, I-20133 Milano, Italy
[27]Jodrell Bank Centre for Astrophysics, Alan Turing Building, School of Physics and Astronomy, The University of Manchester, Oxford Road, Manchester M13 9PL, U.K.
[28]Department of Physics & Astronomy, Tufts University, 574 Boston Avenue, Medford, MA, USA
[29]SISSA, Via Bonomea 265, 34136, Trieste, Italy
[30]Computational Cosmology Center, Lawrence Berkeley National Laboratory, Berkeley, California, U.S.A.
[31]Institut d' Astrophysique de Paris (UMR7095: CNRS & UPMC-Sorbonne Universities), F-75014, Paris, France
[32]Institut d'Astrophysique Spatiale, CNRS, UMR 8617, Université Paris-Sud 11, Bâtiment 121, 91405 Orsay, France
[33]Dipartimento di Fisica e Scienze della Terra, Universitá di Ferrara, Via Giuseppe Saragat 1, I-44122 Ferrara, Italy
[34]Dipartimento di Fisica, Universitá di Roma La Sapienza , P.le A. Moro 2, 00185 Roma, Italy
[35]Dipartimento di Fisica, Universitá di Roma Tor Vergata, Via della Ricerca Scientifica 1, I-00133, Roma, Italy
[36]INFN, Sezione di Roma 2, Via della Ricerca Scientifica 1, I-00133, Roma, Italy
[37]CAS Key Laboratory for Research in Galaxies and Cosmology, Department of Astronomy, University of Science and Technology of China, Hefei, Anhui 230026, China
[38]Institut Néel, CNRS and Université Grenoble Alpes, F-38042 Grenoble, France
[39]Institute of Astrophysics and Space Sciences, University of Lisbon, Tapada da Ajuda, 1349-018 Lisbon, Portugal
[40]Istituto di Fotonica e Nanotecnologie - CNR, Via Cineto Romano 42, I-00156 Roma, Italy
[41]INFN, Sezione di Roma, P.le A. Moro 2, 00185 Roma, Italy
[42]STFC - RAL Space - Rutherford Appleton Laboratory, Harwell, Oxford OX11 0QX, UK
[43]Sorbonne Universités, Institut Lagrange de Paris (ILP), F-75014, Paris, France
[44]IFCA, Instituto de Física de Cantabria (UC-CSIC), Av. de Los Castros s/n, 39005 Santander, Spain
[45]Miller Institute for Basic Research in Science, University of California, Berkeley, CA, 94720, USA
[46]INFN, Sezione di Ferrara, Via Saragat 1, 44122 Ferrara, Italy
[47]Instituto de Astrofísica de Canarias, C/Vía Láctea s/n, La Laguna, Tenerife, Spain
[48]Departamento de Astrofísica, Universidad de La Laguna (ULL), La Laguna, Tenerife, 38206 Spain
[49]The Oskar Klein Centre for Cosmoparticle Physics, Department of Physics, Stockholm University, AlbaNova, SE-106 91 Stockholm, Sweden
[50]The Nordic Institute for Theoretical Physics (NORDITA), Roslagstullsbacken 23, SE-106 91 Stockholm, Sweden
[51]Departamento de Física, Universidad de Oviedo, C. Calvo Sotelo s/n, 33007 Oviedo, Spain
[52]Faculty of Physics, Ludwig-Maximilians Universität, Scheinerstrasse 1, D-81679 Munich, Germany

[53]Excellence Cluster Universe, Boltzmannstr. 2, D-85748 Garching, Germany
[54]Imperial College London, Astrophysics group, Blackett Laboratory, Prince Consort Road, London SW7 2AZ, U.K.
[55]School of Physics and Astronomy and Minnesota Institute for Astrophysics, University of Minnesota/Twin Cities, USA
[56]Centro de Estudios de Física del Cosmos de Aragón (CEFCA), Plaza San Juan, 1, planta 2, E-44001, Teruel, Spain
[57]Department of Physics, Gustaf Hällströmin katu 2a, University of Helsinki, Helsinki, Finland
[58]Helsinki Institute of Physics, Gustaf Hällströmin katu 2, University of Helsinki, Helsinki, Finland
[59]Département de Physique Théorique and Center for Astroparticle Physics, Université de Genève, 24 quai Ansermet, CH–1211 Genève 4, Switzerland
[60]European Space Agency, ESAC, Planck Science Office, Camino bajo del Castillo, s/n, Urbanización Villafranca del Castillo, Villanueva de la Cañada, Madrid, Spain
[61]Centro de Astrofísica da Universidade do Porto and IA-Porto, Rua das Estrelas, 4150-762 Porto, Portugal
[62]Department of Experimental Physics, Maynooth University, Maynooth, Co. Kildare, W23 F2H6, Ireland
[63]CEA Saclay, DRF/Irfu/SPP, 91191 Gif-sur-Yvette Cedex, France
[64]Departamento de Física Quàntica i Astrofísica i Institut de Ciències del Cosmos, Universitat de Barcelona, Martíi Franquès 1, 08028 Barcelona, Spain
[65]Agenzia Spaziale Italiana Science Data Center, Via del Politecnico snc, 00133, Roma, Italy
[66]INAF - Osservatorio Astronomico di Roma, via di Frascati 33, Monte Porzio Catone, Italy
[67]National Center for Nuclear Research, ul. Hoża 69, 00-681 Warsaw, Poland, and The Astronomical Observatory of the Jagiellonian University, ul. Orla 171, 30-244 Kraków, Poland
[68]LAPTh, Université Savoie Mont Blanc & CNRS, BP 110, F-74941 Annecy-le-Vieux Cedex, France
[69]Instituto de Física, Universidade Federal do Rio de Janeiro, 21941-972, Rio de Janeiro, Brazil
[70]Observatório do Valongo, Universidade Federal do Rio de Janeiro, Ladeira Pedro Antonio 43, 20080-090, Rio de Janeiro, Brazil
[71]LPNHE, CNRS-IN2P3 and Universités Paris 6 & 7, 4 place Jussieu F-75252 Paris, Cedex 05, France
[72]SRON (Netherlands Institute for Space Research), Sorbonnelaan 2, 3584 CA Utrecht, The Netherlands
[73]Terahertz Sensing Group, Delft University of Technology, Mekelweg 1, 2628 CD Delft, The Netherlands
[74]Laboratoire de Physique Théorique (UMR 8627), CNRS, Université Paris-Sud, Université Paris Saclay, Bâtiment 210, 91405 Orsay Cedex, France
[75]Institute of Cosmology and Gravitation, University of Portsmouth, Dennis Sciama Building, Burnaby Road, Portsmouth PO1 3FX, United Kingdom
[76]Dipartimento di Fisica, Universitá di Milano Bicocca, Milano, Italy
[77]INFN, sezione di Milano Bicocca, Milano, Italy

E-mail: a.d.challinor@ast.cam.ac.uk

Abstract. Lensing of the cosmic microwave background (CMB) is now a well-developed probe of the clustering of the large-scale mass distribution over a broad range of redshifts. By exploiting the non-Gaussian imprints of lensing in the polarization of the CMB, the *CORE* mission will allow production of a clean map of the lensing deflections over nearly the full-sky. The number of high-S/N modes in this map will exceed current CMB lensing maps by a factor of 40, and the measurement will be sample-variance limited on all scales where linear theory is valid. Here, we summarise this mission product and discuss the science that will follow from its power spectrum and the cross-correlation with other clustering data. For example, the summed mass of neutrinos will be determined to an accuracy of 17 meV combining *CORE* lensing and CMB two-point information with contemporaneous measurements of the baryon acoustic oscillation feature in the clustering of galaxies, three times smaller than the minimum total mass allowed by neutrino oscillation measurements. Lensing has applications across many other science goals of *CORE*, including the search for B-mode polarization from primordial gravitational waves. Here, lens-induced B-modes will dominate over instrument noise, limiting constraints on the power spectrum amplitude of primordial gravitational waves. With lensing reconstructed by *CORE*, one can "delens" the observed polarization internally, reducing the lensing B-mode power by 60 %. This can be improved to 70 % by combining lensing and measurements of the cosmic infrared background from *CORE*, leading to an improvement of a factor of 2.5 in the error on the amplitude of primordial gravitational waves compared to no delensing (in the null hypothesis of no primordial B-modes). Lensing measurements from *CORE* will allow calibration of the halo masses of the tens of thousands of galaxy clusters that it will find, with constraints dominated by the clean polarization-based estimators. The 19 frequency channels proposed for *CORE* will allow accurate removal of Galactic emission from CMB maps. We present initial findings that show that residual Galactic foreground contamination will not be a significant source of bias for lensing power spectrum measurements with *CORE*.

Contents

1 Introduction

The cosmic microwave background (CMB) is gravitationally lensed by large-scale structure as it propagates from the last-scattering surface, leading to a subtle remapping of the temperature and polarization anisotropies (e.g., Ref. [1]). Lensing imprints information in the CMB about the geometry of our Universe and the late-time clustering of matter. This information is otherwise degenerate in the primary CMB fluctuations that are generated at last scattering [2]. The lensing deflection field can be reconstructed using sensitive, high-resolution observations, potentially providing a large-scale, nearly full-sky map of the integrated mass in the entire visible Universe. The power spectrum of this map, when combined with the power spectra of the temperature and polarization anisotropies, constrains parameters such as the (summed) mass of neutrinos and spatial curvature using the CMB alone [3, 4]. Lensing is sensitive to all matter along the line of sight, and not just the luminous matter probed, for example, by galaxy redshift surveys. CMB lensing is therefore highly complementary to other tracers of large-scale structure. For instance, by cross-correlating one can calibrate the astrophysical and instrumental bias relations between the tracers and the underlying density field, which is critical to maximize the returns from future surveys (see e.g., Ref. [5]). Furthermore, the reconstructed lensing map can be used to remove partly the effects of lensing,

which would otherwise obscure our view of the primary fluctuations. A particularly important application of such "delensing" is in the search for primordial gravitational waves via large-angle B-mode polarization, where it can provide critical improvements in primordial constraints [6–8].

In the past decade, CMB lensing has gone from its first detection [9, 10] to becoming a well-established, precision probe of clustering. Reconstructed maps of the CMB lensing deflections have been made with data from ground-based instruments (e.g., Refs. [11–15]) and from the *Planck* satellite [4, 16]. Due to its nearly full-sky coverage, the *Planck* lensing results currently have the greatest statistical power but are very far from exhausting the information available in the lensed CMB. For this reason, lensing is a major goal being targeted by nearly all forthcoming and proposed experiments. These include the Cosmic Origins Explorer (*CORE*), a satellite mission recently proposed to the European Space Agency's fifth call for a medium-class mission.

This paper is one of a series written as part of the development of the *CORE* mission concept and science case. Here, we describe how a full-sky CMB lensing map can be reconstructed with *CORE* data, quantify the expected statistical precision of this map, and illustrate its application across several of the key science targets of the mission. Most of our forecasted results are presented for the baseline mission concept, described in detail elsewhere in this series [17]. However, in some places we present parametric comparisons of different options to justify design choices made in the baseline. Lensing impacts much of *CORE* science; closely related papers in this series describe constraints on inflation [18] (where delensing is significant), cosmological parameters [19] (which combines the temperature, polarization, and lensing power spectra), and galaxy cluster science [20] (where mass calibration with CMB lensing of temperature anisotropies is discussed).

This paper is organised as follows. Section 2 introduces lensing reconstruction and reviews the current observational status. Some further technical details are summarised in Appendix A. Lensing reconstruction with *CORE* is described in Sec. 3. CMB lensing is expected to be a particularly clean probe of the absolute mass scale of neutrinos, through the impact of their mass on the growth of cosmic structure; this important target for *CORE* is discussed in Sec. 4. In Sec. 5, we outline the complementarity between CMB lensing and other tracers of large-scale structure and forecast the improvements that would arise from combining lensing from *CORE* data with contemporaneous large-scale structure surveys. Delensing of B-mode polarization is discussed in Sec. 6 and the implications for constraining primordial gravitational waves are reviewed. In Sec. 7 we highlight the potential for *CORE* to self-calibrate the masses of its cluster catalogue via lensing of CMB polarization, extending the temperature-based forecasts presented in Ref. [20]. While most of the forecasts throughout this paper assume that the 19 frequency channels of *CORE* will allow accurate cleaning of Galactic foreground emission, and so ignore potential Galactic residuals, in Sec. 8 we relax this assumption. We present initial results, based on simulated maps of the polarized Galactic dust emission, on the bias that can arise in the lensing power spectrum from temperature- and polarization-based reconstructions in the pessimistic scenario that dust cleaning is ineffective.

2 CMB lensing reconstruction

Lensing by large-scale structure remaps the CMB temperature and polarization fluctuations imprinted on the last-scattering surface. The lenses lie at all redshifts back to last-scattering,

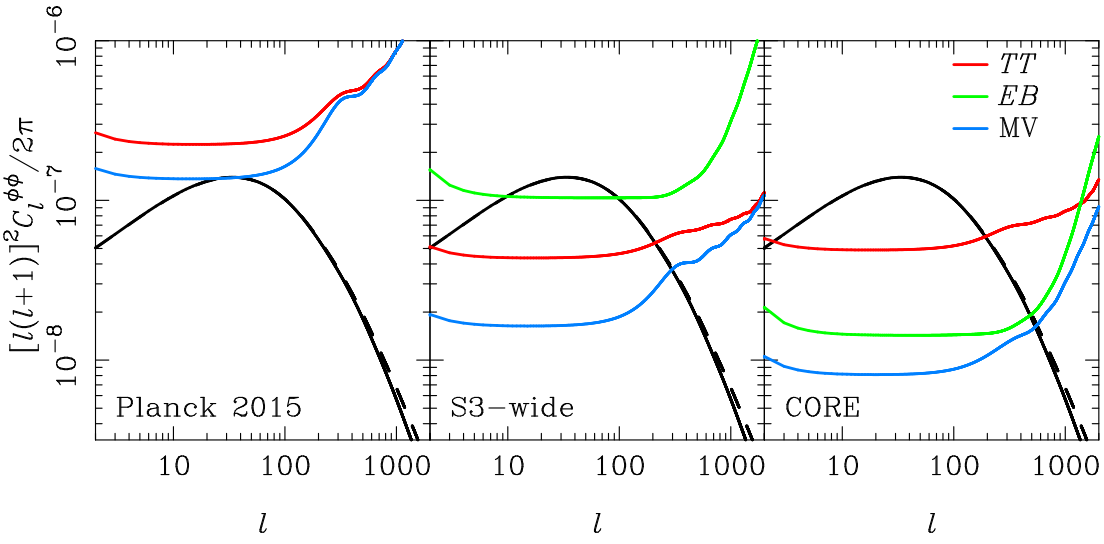

Figure 1. Reconstruction noise of the lensing deflection power spectrum from *Planck* 2015 (left) and as forecast for S3-wide (middle) and *CORE* (right). S3-wide represents a third-generation wide-area (sky fraction of around 40 %) ground-based experiment, with specifications similar to AdvACT. In particular, we follow [21] by assuming a beam size of 1.4 arcmin, a temperature sensitivity of 8.0 μK arcmin and polarization sensitivity of 11.3 μK arcmin. The deflection power spectrum is plotted based on the linear matter power spectrum (black solid) and with nonlinear corrections (black dashed).

but the peak lensing efficiency is around $z = 2$. Large-scale lenses, with $k \lesssim 0.01\,\mathrm{Mpc}^{-1}$, dominate the lensing signal except on the smallest angular scales, making CMB lensing a particularly powerful probe of $O(100)$ Mpc structures at high redshift. The lensing deflections are small, with r.m.s. of 2.5 arcmin, but are coherent over several degrees. To an excellent approximation, the deflection field can be expressed as the angular gradient of the *CMB lensing potential* ϕ, which is itself an integral of the $3D$ gravitational potential along the (background) line of sight. The angular power spectrum of the deflection field, $l(l+1)C_l^{\phi\phi}$, is shown in Fig. 1.

Lensing has several observable effects on the CMB (see Refs. [1, 22] for reviews). It smooths out the acoustic peaks in the temperature and E-mode polarization power spectra and transfers power from large to small scales. This peak smoothing is routinely included when deriving cosmological parameter constraints from the CMB power spectra and the effect itself is detected at more than $10\,\sigma$ in the measurements of the TT power spectrum from *Planck* [23]. Lensing also partially converts E-mode polarization into B-mode [24]. These lens-induced B-modes have an almost white-noise spectrum, corresponding to around 5 μK arcmin of noise, on the large angular scales relevant for searches for primordial B-mode polarization sourced by a stochastic background of primordial gravitational waves (see Sec. 6). Finally, lensing induces non-Gaussianity in the CMB, which shows up as higher-order non-zero connected moments (in particular the trispectrum or connected 4-point function) and as non-zero 3-point correlator between pairs of CMB fields and tracers of large-scale structure [25, 26].

Exploitation of the non-Gaussianity induced by lensing can be conveniently thought of as a two-step process. The first involves *lens reconstruction*, whereby an estimate for the lensing potential ϕ is obtained from quadratic combinations of the observed CMB fields [27].

In the second step, the lens reconstruction is correlated with itself, to estimate the lensing potential power spectrum $C_l^{\phi\phi}$, or an external tracer of large-scale structure, to estimate the correlation between the lensing potential and the tracer. The process of lens reconstruction can be understood by noting that for fixed ϕ, lensing induces anisotropic 2-point correlations in the CMB. The linear response of the covariance between lensed CMB fields $\tilde{X}_{lm}$ and $\tilde{Y}_{lm}$, where X and $Y = T$, E, or B, to a variation in the lensing potential is

$$\langle \delta(\tilde{X}_{l_1 m_1} \tilde{Y}_{l_2 m_2}) \rangle \approx \sum_{LM} (-1)^M \begin{pmatrix} l_1 & l_2 & L \\ m_1 & m_2 & -M \end{pmatrix} \mathcal{W}^{XY}_{l_1 l_2 L} \delta\phi_{LM} \,, \tag{2.1}$$

where the covariance response functions $\mathcal{W}^{XY}_{l_1 l_2 L}$ are given in Appendix A (see also Ref. [28]). An optimal quadratic estimator $\hat{\phi}_{LM}$ can be written in the form[1]

$$\hat{\phi}^{XY}_{LM} = \frac{(-1)^M}{2} \frac{1}{\mathcal{R}^{XY}_L} \sum_{l_1 m_1, l_2 m_2} \begin{pmatrix} l_1 & l_2 & L \\ m_1 & m_2 & -M \end{pmatrix} [\mathcal{W}^{XY}_{l_1 l_2 L}]^* \bar{X}_{l_1 m_1} \bar{Y}_{l_2 m_2} \,, \tag{2.2}$$

where $\bar{X}$ and $\bar{Y}$ are the inverse-variance filtered fields and the normalisation $\mathcal{R}^{XY}_L$ is chosen to ensure the estimator is unbiased. The individual quadratic estimators can be combined linearly to give a minimum-variance (MV) combination: $\hat{\phi}^{MV}_{LM} = \sum_{XY} \hat{\phi}^{XY}_{LM} \mathcal{R}^{XY}_L / \sum_{XY} \mathcal{R}^{XY}_L$.

Lens reconstruction is statistical, with Gaussian fluctuations of the CMB giving rise to a statistical noise in the reconstruction. This reconstruction noise is similar to shape noise in galaxy lensing, whereby the intrinsic ellipticity of a galaxy adds white noise to the estimated gravitational shear. The reconstruction noise can be quantified by its power spectrum, usually denoted $N^{(0)}_L$. Consider forming the power spectrum of $\hat{\phi}^{XY}_{LM}$. This is quartic in the CMB fields and the connected part of this 4-point function gives simply $C^{\phi\phi}_L$ (plus an additional non-local coupling to the potential power spectrum, $N^{(1)}_L$, which arises from non-primary couplings [26, 29]) while the disconnected part gives $N^{(0)}_L$. The lens reconstruction has high S/N on scales where $C^{\phi\phi}_L \gg N^{(0)}_L$. Examples of $N^{(0)}_L$ for various experiments are given in Fig. 1.

CMB lensing is a rapidly advancing frontier of observational cosmology. Estimates of the lensing potential power spectrum from the CMB 4-point function from *Planck*, and several ground-based experiments, are shown in Fig. 2. The *Planck* results [4] provide the highest S/N detection of CMB lensing to date (around $40\,\sigma$). At the noise levels of *Planck* (around $30\,\mu$K arcmin in temperature), the TT estimator has the highest S/N and dominates the MV combination, as shown in the left-hand panel of Fig. 1. On large angular scales, the reconstruction noise power is approximately [30]

$$[L(L+1)]^2 N^{(0)}_L \approx \left\{ \frac{1}{8} \sum_l \frac{2l+1}{4\pi} \left(\frac{C^{TT}_l}{C^{TT}_{l,\mathrm{tot}}} \right)^2 \left[\left(\frac{d \ln \mathcal{D}^{TT}_l}{d \ln l} \right)^2 + \frac{1}{2} \left(\frac{d \ln C^{TT}_l}{d \ln l} \right)^2 \right] \right\}^{-1} , \tag{2.3}$$

where C^{XY}_l is the (lensed) CMB power spectrum between fields X and Y, C^{XY}_l is the total spectrum including (beam-deconvolved) instrument noise for $X = Y$, and $\mathcal{D}^{XY}_l \equiv l(l+1)C^{XY}_l/(2\pi)$. The power spectrum $L^2(L+1)^2 N^{(0)}_L/4$ is approximately constant on

[1] Generally, it is necessary also to subtract a *mean field* term from the estimator to deal with survey anisotropies such as masking and anisotropic instrument noise and filtering.

large scales corresponding to white noise in the reconstructed convergence ($\kappa = -\nabla^2\phi/2$) or shear ($\gamma = -\eth^2\phi/2$). This behaviour arises since for large-scale lenses, the convergence and shear are reconstructed locally from much smaller-scale CMB anisotropies. The convergence produces dilation of the local small-scale CMB power spectrum, while the shear produces local anisotropy. It can be shown that the term involving $d\ln\mathcal{D}_l^{TT}/d\ln l$ in Eq. (2.3) is the information from the convergence (and so vanishes for a scale-invariant spectrum $\mathcal{D}_l^{TT} =$ const.), while the term involving $d\ln C_l^{TT}/d\ln l$ is the information from the shear [31].

While the S/N of the TT estimator can be improved by increasing the resolution and sensitivity beyond *Planck*, it can never exceed unity for scales smaller than multipole $L \approx 200$. Furthermore, extragalactic foregrounds make using the temperature anisotropies very difficult at scales $l > 2500$. Rather, the way to improve lensing reconstructions significantly is to use high-sensitivity polarization observations [32]. In particular, if the lens-induced B modes can be mapped with high S/N, the EB estimator becomes the most powerful. On large angular scales, the reconstruction noise power for this estimator is approximately (for $L \geq 2$)

$$L^4 N_L^{(0)} \approx \left(\frac{1}{2} \sum_l \frac{2l+1}{4\pi} \frac{(C_l^{EE})^2}{C_{l,\mathrm{tot}}^{EE} C_{l,\mathrm{tot}}^{BB}} \right)^{-1} , \tag{2.4}$$

and is limited by the total B-mode power $C_{l,\mathrm{tot}}^{BB}$ (including instrument noise), which can be very small for low-noise observations. The EB estimator for large scale lenses is only sensitive to shear as the dilation of small-scale polarization by a constant convergence does not convert E-mode polarization into B-mode.[2] Polarization-based lens reconstructions have been demonstrated recently from ground-based experiments [11–14], and also *Planck*, but are currently very noisy. Future, funded wide-area CMB surveys (see S3-wide in Fig. 1, which has specifications similar to AdvACT) also do not have the sensitivity to exploit polarization-based lensing fully. To image the lens-induced B-modes requires the polarization noise level to be well below $5\,\mu$K arcmin. Achieving such sensitivity over a large fraction of the sky – to maximise the number of resolved lensing modes and the overlap with large-scale structure surveys – would require a ground-based experiment with around 5×10^5 detectors. Plans for such a programme, CMB-S4, are currently under development [33]. Alternatively, the same goal can be reached with almost two orders of magnitude fewer detectors from a space-based experiment, as we discuss in Sec. 3.

Finally, we note that at very low noise levels it is possible to improve over lens reconstructions based on quadratic estimators (e.g., Refs. [34–37]). For example, we see from Eq. (2.4) that the precision of the EB estimator is limited at low noise levels by the small-scale lens-induced B-mode power. However, simple field counting suggests that with no noise we should be able to invert the observed E- and B-fields to recover the unlensed E-modes and the lensing potential ϕ. For the noise levels of *CORE*, the improvement from more optimal estimators is rather modest and so, for simplicity, most of the forecasts in this paper are based on quadratic estimators. However, in Sec. 6 we do discuss further the improvements in constraints on primordial gravitational waves that arise from delensing with a more optimal lens reconstruction.

[2] Indeed, the reconstruction noise on the EB estimator is very large at $L = 1$ since the dipole of the lensing potential produces no shear.

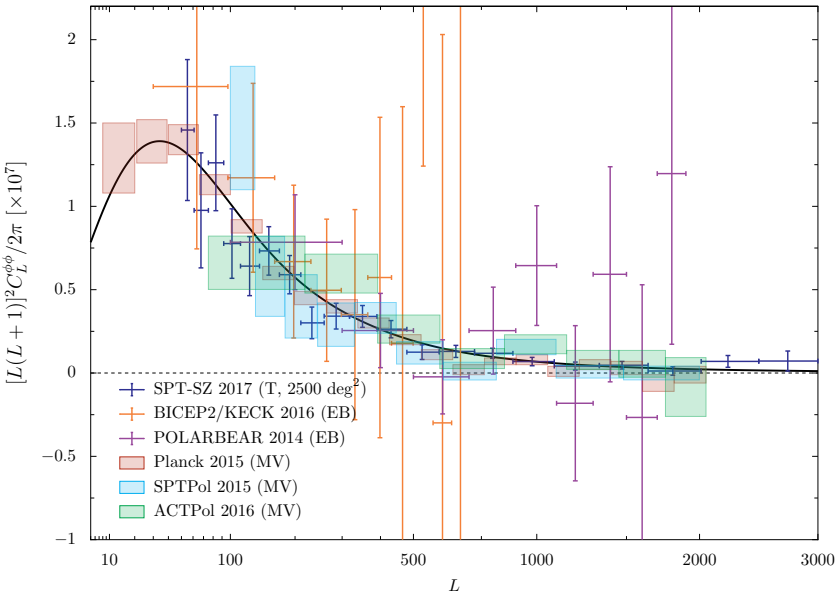

Figure 2. Current lensing potential power spectrum measurements from *Planck* 2015 [4], SPTpol [12], POLARBEAR [11], ACTPol [13], BICEP2/Keck Array [14], and SPT-SZ [15].

3 Lens reconstruction with *CORE*

The baseline configuration for the *CORE* mission is summarised in Table 1 of Ref. [17]. Briefly, it consists of 19 frequency channels in the range 60–600 GHz with beam sizes (full width at half-maximum) ranging from 18 arcmin (at 60 GHz) to 2 arcmin (at 600 GHz). For the forecasts in this paper, we combine the six channels in the frequency range 130–220 GHz with inverse-variance noise weighting, assuming that the channels outside this range can be used to clean Galactic foregrounds without further significant loss of sensitivity. The polarization sensitivity of each of the six "CMB" channels is around 5 μK arcmin in polarization (and a factor $\sqrt{2}$ better in temperature) assuming a four-year mission. The combination of the CMB channels gives a polarization sensitivity of 2.1 μK arcmin and an effective resolution of around 6.2 arcmin.

The polarization noise power spectrum of the combination of the six CMB channels is shown in Fig. 3, where it is compared to the CMB TT, EE, and BB power spectra from curvature fluctuations and from primordial gravitational waves with a tensor-to-scalar ratio $r = 0.01$. We see that with *CORE*, the E-mode polarization has $S/N > 1$ for multipoles $l < 2000$ and the lens-induced B-modes have $S/N > 1$ for $l < 1000$. Figure 3 also compares the noise power to that of the full *Planck* survey; *CORE* has around 30 times the polarization sensitivity of *Planck*.

The noise levels $N_L^{(0)}$ on lens reconstructions from *CORE* in its baseline configuration are shown in the right-hand panel of Fig. 1 for a temperature-based quadratic estimator, the EB estimator, and the minimum-variance combination of all five quadratic estimators. The EB estimator is the most powerful quadratic estimator since, as noted above, *CORE*'s polarization sensitivity of 2.1 μK arcmin and angular resolution allow imaging of the lens-induced B-modes. This situation is quite different from *Planck*, and from the current generation of wide-area surveys (see S3-wide in Fig. 1). For these, lensing reconstruction is dominated by

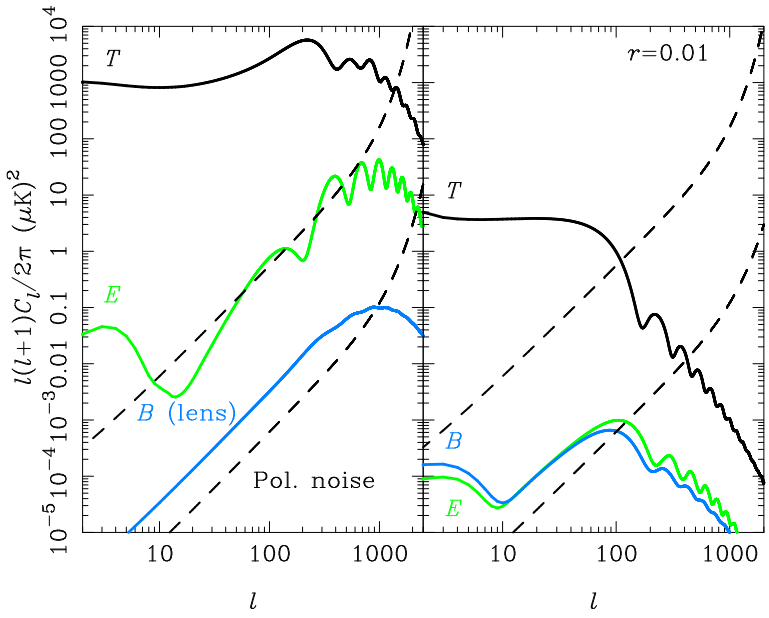

Figure 3. Power spectra of the polarization noise for *CORE* (lower dashed lines) and *Planck* 2015 (upper dashed lines) compared to the TT (black), EE (green), and BB (blue) power spectra from curvature perturbations (left) and gravitational waves for $r = 0.01$ (right).

the TT estimator. This transition to the regime where EB dominates is transformational for two reasons. First, only then is it possible to achieve high S/N reconstructions of lenses at multipoles $L > 200$ and so maximise the cosmological information that can be extracted from CMB lensing. Second, the non-Gaussian nature of extragalactic foregrounds to the temperature anisotropies (e.g., radio and infrared galaxies and the thermal Sunyaev-Zel'dovich signal from galaxy clusters) can bias estimation of the lensing power spectrum and generally requires correction [38]. However, lens reconstructions based on polarization are expected to be much cleaner than those from temperature [39].

We see from Fig. 1 that *CORE* will reconstruct lensing with $S/N > 1$ *per mode* up to multipoles $L \approx 550$ over nearly the full sky. Significantly, *CORE* can extract essentially all of the information in the lensing power spectrum on scales where linear theory is reliable. A useful way to summarise the information content of the lens reconstruction is through the total S/N of a measurement of the amplitude of the lensing power spectrum, i.e.,

$$\left(\frac{S}{N}\right)^2 \approx f_{\rm sky} \sum_L \frac{2L+1}{2} \left(\frac{C_L^{\phi\phi}}{C_L^{\phi\phi} + N_L^{(0)}}\right)^2 , \tag{3.1}$$

where $f_{\rm sky}$ is the fraction of the sky that is usable for lensing science with the survey. Based on experience with *Planck*, we expect $f_{\rm sky} \approx 0.7$ for *CORE*. Note that $(S/N)^2$ is just half the effective number of modes in the reconstruction and so we define $N_{\rm modes} \equiv 2(S/N)^2$. For *CORE*, $N_{\rm modes} \approx 1.6 \times 10^5$; for comparison,

$$N_{\rm modes} = \begin{cases} 4.0 \times 10^3 & \textit{Planck}\ 2015 \\ 3.9 \times 10^4 & \text{S3-wide} \\ 1.6 \times 10^5 & \textit{CORE}\,, \end{cases} \tag{3.2}$$

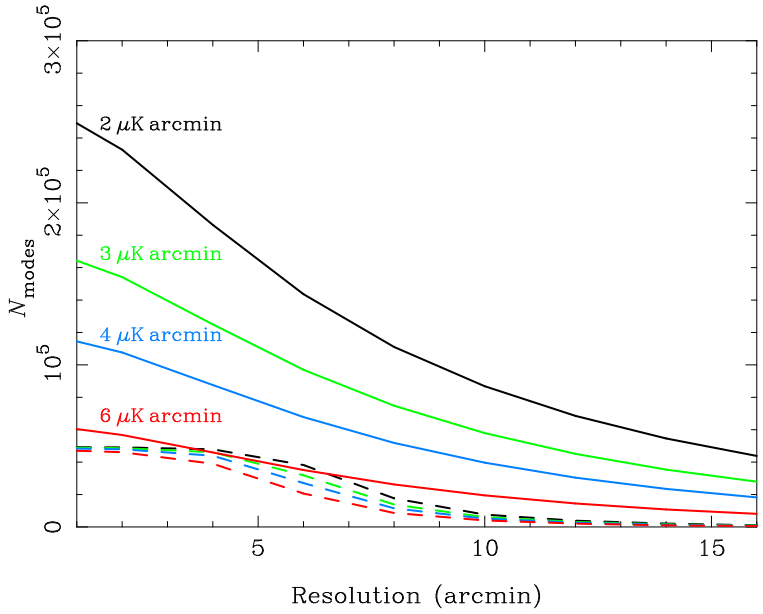

Figure 4. Number of effective resolved lensing reconstruction modes as a function of angular resolution for surveys covering 70 % of the sky for the indicated polarization noise levels. The solid lines are for the EB quadratic estimator while the dashed lines are for TT. In all cases, CMB modes are only used up to $l_{\rm max} = 3000$ in the quadratic estimators.

assuming S3-wide can use 40 % of the sky. Figure 4 shows $N_{\rm modes}$ for 70 % sky coverage as a function of angular resolution for polarization noise levels in the range 2–6 μK arcmin. For polarization noise better than 5 μK arcmin (i.e., levels where imaging of the lens-induced B-modes becomes possible), the EB estimator indeed dominates $N_{\rm modes}$. The number of lensing modes from the EB estimator continues to increase with decreasing noise levels as B-modes on smaller scales (where the lens-induced B-mode power is not white) are imaged. Note, however, that increasing $N_{\rm modes}$ does not necessarily lead to improved parameter constraints from the lensing spectrum as these can rather be limited by parameter degeneracies (see Sec. 4 for the case of neutrino masses).

4 Absolute neutrino mass scale

Several aspects of the neutrino sector are still not well understood. In particular, neutrino oscillations show that neutrinos must be massive, with the flavour eigenstates a mixture of mass eigenstates. Oscillations are sensitive to the differences of the squared masses, but not to the absolute mass scale. Since neutrinos are so numerous, even small masses can have a significant cosmological effect making *CORE* a powerful probe of their unknown absolute mass scale. In addition, the usual assumption that the three active flavour states (i.e., those that participate in the weak interaction) mix with three mass eigenstates has been questioned in light of a number of anomalies found with short-baseline oscillation and reactor measurements (see Ref. [40] for a review). Instead, one or more additional sterile neutrinos can be introduced, which do not participate in weak interactions, and that, alongside the active states, mix with four or more mass eigenstates. Sterile–active mass splittings at the eV scale are required to resolve the above anomalies, but are disfavoured by current cosmological

bounds (e.g., Ref. [23]). CMB data are sensitive to the mass of sterile neutrinos through lensing, while the damping tails of the temperature and polarization power spectra provide sensitivity to their effective number.

4.1 Masses of active neutrinos

Neutrino oscillation data show that neutrinos must be massive, but the data are insensitive to the absolute neutrino mass scale. Cosmological observations are naturally complementary since they are sensitive mostly to the total mass with only weak sensitivity to the mass splittings. The mass splittings inferred from oscillations, $m_2^2 - m_1^2 = (7.53 \pm 0.18) \times 10^{-5}\,\mathrm{eV}^2$ and $|m_3^2 - m_2^2| = (2.44 \pm 0.06) \times 10^{-3}\,\mathrm{eV}^2$ [41], imply two possible mass orderings: the normal ordering ($m_3 > m_2 > m_1$) with a minimum total mass of $\sum m_\nu \approx 59\,\mathrm{meV}$; and the inverted ordering ($m_2 > m_1 > m_3$) with a minimum total mass of 98 meV. The mass scale can also be probed kinematically with laboratory β-decay experiments. At the target minimal-mass scales, the effective masses that are probed with such experiments are well below the detection limits of current and future planned experiments. However, next-generation searches for neutrinoless double beta decay (which would require neutrinos to be Majorana particles) are expected to reach sensitivities to the relevant effective mass that could allow detection if the ordering is inverted (e.g., Ref. [42]).

Neutrinos with masses less than around 0.5 eV were still relativistic around the time of recombination. Their effect on the *primary* CMB anisotropies is therefore limited to projection effects due to the change in the angular diameter distance to last scattering. If we keep the physical densities of CDM, baryons and dark energy fixed, an increase in the neutrino mass increases the expansion rate after neutrinos become non-relativistic. The associated reduction in the angular diameter distance to last scattering can be offset by a reduction in the dark energy density (or, equivalently, the Hubble constant). This geometric degeneracy limits our ability to probe lighter neutrino masses with the primary CMB anisotropies alone; for example, the 95 % upper limit on the summed neutrino mass from *Planck* temperature and polarization anisotropies is $\sum m_\nu < 0.49\,\mathrm{eV}$ [23]. However, the modification to the expansion rate affects geometric probes, such as the measurement of the baryon acoustic oscillation (BAO) feature in the clustering of galaxies, which can be used to break the CMB geometric degeneracy. For example, combining *Planck* with current BAO data improves the constraint to around $\sum m_\nu < 0.2\,\mathrm{eV}$ [23, 43]. In models with curvature or dynamical dark energy the geometric degeneracy is further exacerbated and the constraints on $\sum m_\nu$ are weakened.

Massive neutrinos also affect the growth of structure on scales smaller than the horizon size when neutrinos become non-relativistic, leaving a distinctive feature in the lensing potential power spectrum. Massive neutrinos can only cluster on scales larger than their free-streaming scale, roughly the product of their r.m.s. speed and the Hubble time. Once neutrinos become non-relativistic, their comoving free-streaming scale *decreases* with time as their r.m.s. speed falls as $1/a$, where a is the scale factor. For reference, at redshift $z = 2$ where the kernel for CMB lensing peaks, the associated comoving wavenumber is $k_{\mathrm{fs}} \approx 0.09(m_\nu/50\,\mathrm{meV})\,\mathrm{Mpc}^{-1}$ – see, for example, Ref. [44] – corresponding to a multipole $l \approx 60$ for $m_\nu = 50\,\mathrm{meV}$ (see, e.g., Ref. [44]). The increase in the expansion rate due to non-relativistic massive neutrinos slows the growth of structure in the other matter components on scales smaller than the free-streaming scale. At any given redshift, the net effect in the power spectrum of the gravitational potential is an almost constant fractional suppression for $k > k_{\mathrm{fs}}(a)$. Scales larger than the horizon size at the non-relativistic transition are not

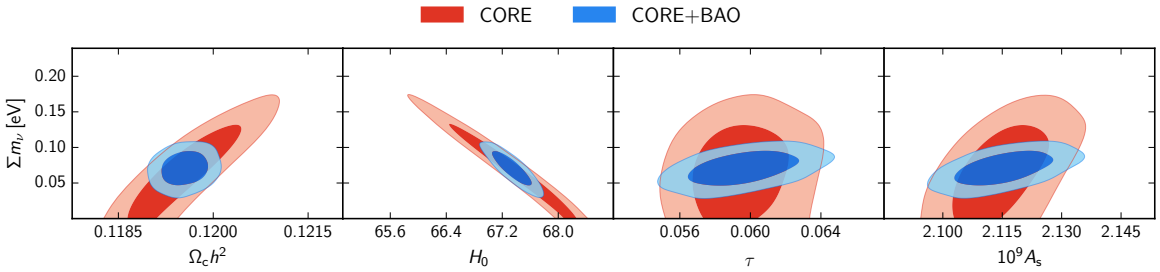

Figure 5. Two-dimensional marginalised constraints (68 % and 95 %) in ΛCDM models with massive neutrinos for *CORE* (red) and the combination of *CORE* and future BAO measurements from DESI and *Euclid* (blue). The fiducial model has the minimal masses in the normal ordering with a summed mass $\sum m_\nu = 60\,\mathrm{meV}$.

suppressed since neutrinos have always clustered on such scales, mitigating the effect of the enhanced expansion rate on the growth of structure. For a given mass, the amount of suppression in the lensing potential power spectrum $C_l^{\phi\phi}$ depends on exactly which other parameters are held fixed. For example, moving along the geometric degeneracy of the primary CMB anisotropies (i.e., fixing the physical densities in CDM and baryons, the angular-diameter distance to last scattering, the primordial power spectrum and the optical depth to reionization), $C_l^{\phi\phi}$ is suppressed by around 1.5 % for a total mass $\sum m_\nu = 0.06\,\mathrm{eV}$ compared to the massless case. By way of comparison, the amplitude of the lensing potential power spectrum can be measured with a $1\,\sigma$ error of around 0.35 % with *CORE*, although, as we shall see below, this does not translate directly into a constraint on the summed neutrino mass due to parameter degeneracies.

Figure 5 shows forecasted parameter constraints from *CORE* combining the temperature and polarization power spectrum measurements with the lensing potential power spectrum obtained from the minimum-variance quadratic estimator. The fiducial model is close to the minimal-mass in the normal ordering, with $\sum m_\nu = 60\,\mathrm{meV}$, and the analysis is performed assuming degenerate masses.[3] Combining the anisotropy and lensing power spectra of *CORE*, we forecast a $1\,\sigma$ error of 44 meV for the summed mass. This is a significant improvement over current constraints, but falls someway short of the minimum masses inferred from neutrino oscillations.

The constraint on the summed mass from *CORE* alone is limited by degeneracies with other parameters, as shown in Fig. 5. The degeneracy with the Hubble constant arises from the geometric degeneracy in the primary anisotropies. The degeneracy with the physical density in CDM, $\Omega_c h^2$, arises from lensing: an increase in $\Omega_c h^2$ pushes matter–radiation equality to higher redshift, boosting the late-time matter power spectrum as structure has had longer to grow in the matter-dominated era [4, 45]. An increase in $\Omega_c h^2$ can therefore be offset with an increase in the neutrino mass to preserve the lensing power. Finally, an increase in the amplitude A_s of the primordial power spectrum increases the lensing power

[3] Assuming degenerate neutrinos at such low masses is clearly inconsistent with the mass splittings inferred from neutrino oscillations. However, cosmological observations have little sensitivity to the mass splittings and so the constraints on the summed mass are very similar irrespective of whether degenerate masses or masses with realistic splittings are assumed; see Ref. [19] for an explicit demonstration in the context of the *CORE* mission.

spectrum proportionately on all scales, and so is also positively correlated with the neutrino mass.

The constraint on neutrino mass can be significantly improved by combining with measurements of the BAO feature – a purely geometric measurement – in the clustering of galaxies, since these can break the degeneracy between $\Omega_c h^2$ and $\sum m_\nu$. Increasing $\Omega_c h^2$ and $\sum m_\nu$ at fixed angular scale of the CMB acoustic peaks leads to an increase in the radial BAO observable $H(z) r_s(z_{drag})$ at $z > 1$ and a decrease at lower redshift, and an increase in the angular observable $d_A(z)/r_s(z_{drag})$ (see, e.g., Ref. [46]). Here, $r_s(z_{drag})$ is the sound horizon at the drag epoch and $d_A(z)$ is the angular-diameter distance to redshift z. Figure 5 forecasts the effect of combining *CORE* data with BAO data from DESI and *Euclid* in the redshift range $0.15 \leq z \leq 2.05$, using predictions from Ref. [47] for the BAO measurement errors. This combination could shrink the error on $\sum m_\nu$ to 17 meV, giving a high chance of a significant detection (greater than $3\,\sigma$) of non-zero neutrino mass even for the minimal-allowed mass.[4] Furthermore, if the total mass is close to this minimum (around 60 meV), *CORE*+BAO will likely disfavour any total mass allowed by the inverted ordering at greater than $2\,\sigma$ significance, providing important information on the mass orderings.

Neutrino mass determination from CMB lensing relies on comparing the clustering power at low redshift, determined from lensing, with the power at last scattering, determined from the CMB anisotropies. However, scattering at reionization reduces the *observed* anisotropy on scales smaller than the projection of the horizon size there by a factor $e^{-\tau}$, where τ is the optical depth to reionization. It follows that only the combination $A_s e^{-2\tau}$ is measured very precisely from the CMB temperature and polarization power spectra on these scales: the $1\,\sigma$ error from *Planck* is 0.7 % [23] and we forecast 0.2 % for *CORE*. To separate out A_s requires an independent measurement of the optical depth. This can be obtained from the E-mode polarization data at low multipoles, where scattering at reionization generates power giving rise to the characteristic feature in the E-mode power spectrum at $l < 10$ (see Fig. 3). Measuring polarization on such large scales requires a nearly full-sky survey, stable observations over wide separations, and excellent rejection of Galactic foreground emission. To date, such measurements have only been achieved from space (although efforts are underway with the ground-based experiment CLASS [48]). Recent results from *Planck* give $\tau = 0.055 \pm 0.009$ [49], while for *CORE* we forecast a $1\,\sigma$ error of 0.002 equal to the cosmic-variance limit. This precision on τ limits that on A_s to around 0.4 %, and our ability to predict the lensing power spectrum for a given mass is similarly uncertain. If the S/N on a measurement of the amplitude of the lensing power spectrum significantly exceeds $A_s/\sigma(A_s)$, the uncertainty in the neutrino mass determination will be dominated by that in A_s if precision BAO data is used to break the degeneracy with $\Omega_c h^2$. For *CORE*, with $\sigma(\tau) = 0.002$, this corresponds to $N_{modes} \approx 1 \times 10^5$, similar to what is achieved in the baseline configuration. It follows that further improvement in the lensing S/N (i.e., increasing the sensitivity or resolution) would not lead to proportional improvement in the measurement of neutrino mass; see Ref. [19] for explicit comparisons of possible design choices for *CORE*.

To illustrate the importance of precise determination of the optical depth to reionization for neutrino mass constraints, we consider replacing the large-angle polarization data from *CORE* with a *Planck*-like prior with $\sigma(\tau) = 0.01$. In this case, the error on the summed neutrino mass from *CORE*+BAO almost doubles to 30 meV. This situation is similar to that

[4] This constraint is a little better than that reported in Ref. [19] due to our inclusion of *Euclid* BAO data, which helps particularly at higher redshifts ($z > 0.9$).

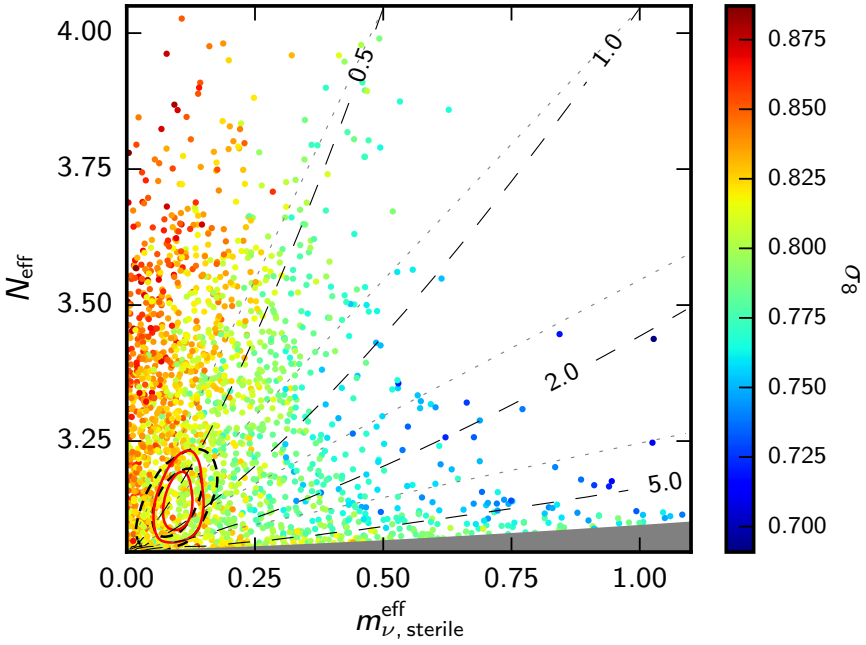

Figure 6. Samples from the current *Planck* temperature and low-l polarization data combined with BAO data (following Ref. [23]) in the $N_{\rm eff}$–$m^{\rm eff}_{\nu,\,\rm sterile}$ plane, colour-coded by σ_8. The models have one massive sterile neutrino family, with effective mass $m^{\rm eff}_{\nu,\,\rm sterile}$, in addition to the three active neutrinos. Dashed contours show forecast 68 % and 95 % constraints from *CORE*, and solid contours the forecast when combining with future BAO data from DESI and *Euclid*. The physical mass of the sterile neutrino in the thermal scenario, $m^{\rm thermal}_{\nu,\rm sterile}$, is constant along the grey dashed lines, with the indicated mass in eV; the grey region shows the region excluded by the prior $m^{\rm thermal}_{\nu,\rm sterile} < 10\,\rm eV$, which excludes most of the region where the neutrinos behave nearly like dark matter.

which CMB-S4 will face in the absence of a contemporaneous space mission if attempts to measure polarization on very large scales from the ground are unsuccessful.

4.2 Sterile neutrinos and other massive additional relic particles

In addition to sterile neutrinos, many extensions to the standard model could also produce additional relic particles, for example thermal or non-thermal distributions of axions or gauge bosons. If they remain relativistic until today, the main effect in the CMB is via the increased expansion rate and anisotropic stress in the early universe [50]. The former reduces power in the damping tail at fixed angular separation of the acoustic peaks, while the anisotropic stress introduces a characteristic phase shift in the acoustic oscillations and hence peak locations. The contribution of non-photonic relativistic particles to the energy density in the early universe is usually parameterised by $N_{\rm eff}$, such that

$$\Delta\rho = \frac{7}{8}\left(\frac{4}{11}\right)^{4/3} N_{\rm eff}\,\rho_\gamma\,, \tag{4.1}$$

where ρ_γ is the energy density of photons. With this parameterisation, the three families of active neutrinos contribute $N_{\rm eff} = 3.046$ and one additional sterile neutrino with the same

thermal distribution function as the active neutrinos would contribute a further $\Delta N_{\rm eff} \approx 1$. The damping tails in the temperature and, particularly, polarization power spectra[5] measured with *CORE* alone gives a forecast error of $\sigma(N_{\rm eff}) \approx 0.04$ [19].

If the relic particles are massive, but are not so massive that they look like cold dark matter in the CMB and lensing (i.e., physical mass less than around 10 eV), *CORE* can constrain both the mass and their contribution to $N_{\rm eff}$. As shown in Fig. 6, *CORE* could dramatically reduce the allowed parameter space compared to current *Planck* constraints. For detectable additional species, we forecast $\sigma(N_{\rm eff}) \approx 0.04$ as for light relics, and a $1\,\sigma$ constraint on $m^{\rm eff}_{\nu,\,\rm sterile} \equiv (94.1\Omega_{\nu,\,\rm sterile}h^2)\,{\rm eV}$ of approximately 0.03 eV (or 0.02 eV including BAO). Here, $\Omega_{\nu,\,\rm sterile}h^2$ is the energy density of the relic today and is proportional to the product of the physical mass and $(\Delta N_{\rm eff})^{3/4}$ for a thermal relic that is now non-relativistic. These constraints are forecast assuming a thermal relic, but *CORE* would give similar constraints on a variety of more general non-thermal models. The forecast error of $\sigma(N_{\rm eff}) \approx 0.04$ would be sufficient to detect at high significance any thermal relics produced after the QCD phase transition (which are currently weakly disfavoured), and is also sufficient to detect some scenarios where multiple new particles decoupled from the standard model at energies above 1 TeV.

5 Combining *CORE* lensing with other probes of clustering

Lensing of the CMB probes the large-scale distribution of matter in all of the observable universe. The same structures at lower redshift that are traced by other cosmological observables, such as the distribution of galaxies and the coherent distortion of the shapes of galaxies by weak gravitational lensing (cosmic shear), also lens the CMB resulting in non-zero correlations between CMB lensing and the tracer. Cross-correlating CMB lensing with large-scale structure tracers is highly complementary to the auto-correlations of each observable. Cross-correlations tend to be more robust, since they are immune to additive systematic effects that are independent between the observables. Moreover, cross-correlating allows calibration of multiplicative effects, such as galaxy bias or multiplicative bias in the estimation of galaxy shapes, which would otherwise compromise the cosmological information that can be extracted from the observable.

CORE will produce a high-S/N lensing map over nearly the full sky, allowing a wealth of cross-correlation science with current and future large-scale structure surveys. In this section, we highlight the potential for cross-correlating CMB lensing from *CORE* with two particularly important tracers: lensing of galaxies and galaxy clustering. We also summarise areas where cross-correlation of lensing and other fields may advance our understanding of astrophysics at high redshift.

5.1 Galaxy lensing

Lensing by large-scale structure can be probed in optical imaging surveys through its shearing effect on the shapes of background galaxies. Galaxy lensing is a key observable of ongoing (e.g., DES [52] and KiDS [53]) and future imaging surveys (e.g., LSST [54] and *Euclid* [55]).

[5]The accuracy of parameter inferences from the temperature power spectrum measured by *Planck* [23] are now close to being limited by errors in the modelling of extragalactic foregrounds. Fortunately, further progress can be made with the polarization anisotropies on small angular scales [51], since the degree of polarization of the anisotropies is relatively larger there (greater than 15 % by $l = 2000$) than the foreground emission.

With approximate redshifts for the source galaxies, it is possible to map the evolution of cosmic shear over time (tomography) and so probe the growth of structure and the cosmic expansion history and hence the physics of cosmic acceleration (see below).

CMB lensing is highly complementary to galaxy lensing. Although the CMB reconstruction is at lower resolution, and lacks the tomographic aspect accessible with galaxy lensing, it probes higher redshifts, and the S/N is dominated by clustering in the well-understood linear regime. By constrast, most of the potential S/N for galaxy lensing is deep in the non-linear regime where modelling uncertainties are larger. Generally, CMB and galaxy lensing are affected by very different systematic effects. For the latter, intrinsic alignments in the shapes of galaxies due to the local tidal environment in which they form (see Ref. [56] for a review), source redshift errors, and biases in the estimation of the shapes of galaxies are all important. In practice, the combination of CMB and galaxy lensing with overlapping footprints on the sky is particularly promising. For example, their cross-correlation allows self-calibration of multiplicative biases in the galaxy shape measurements [5, 57, 58] and models for the intrinsic-alignment signal [59–61]. The correlation between CMB and galaxy lensing has been detected recently at modest significance using a range of surveys [62–66]. With *CORE* and, for example, *Euclid* lensing, the amplitude of the total cross-correlation will be measured with a S/N of around 170. The combination of CMB and galaxy lensing will also yield parameter constraints that are more robust against degeneracies with other parameters. We now illustrate some of these ideas in the context of constraints on neutrino mass and dark energy.

Absolute neutrino masses The constraints on the absolute mass scale of neutrinos from *CORE* (Sec. 4) are comparable to those forecast for other future probes of clustering, including cosmic shear measurements from *Euclid* [55]. Even stronger and, importantly, more robust neutrino mass constraints can be obtained by combining *CORE* with such probes. As an illustration of the robustness against parameter degeneracies, a conservative forecast[6] for the combination of *CORE*, BAO, and *Euclid* cosmic shear in models with spatial curvature gives an error on the summed mass of active neutrinos of less than 20 meV (from 16 meV without free curvature), so at least a $3\,\sigma$ detection of non-zero mass is still likely [19]. In contrast, with current CMB data the degradation would be much worse: for the combination *Planck*+BAO+*Euclid* cosmic shear the degradation in errors when marginalising over free curvature is from 23 meV to 33 meV.

Dark energy and modifications to gravity Understanding the observed late-time accelerated expansion of the Universe is a critical problem for fundamental physics. While current observations are consistent with acceleration being due to a cosmological constant (the ΛCDM model), its unnaturally small value has led to the development of alternative theories such as those involving (dynamical) dark energy or modifications to the laws of gravity on large scales. Probing the underlying physics of cosmic acceleration, through measurements of the expansion history and growth of structure, is a key science goal for Stage-IV dark energy experiments (e.g., DESI, LSST, and *Euclid*). The effects of dark energy are degenerate in the primary CMB fluctuations, which originate at much higher redshift than the onset of cosmic acceleration ($z \approx 1$). However, through secondary effects in the CMB, *CORE* will provide several dark energy observables that complement other low-redshift probes: the

[6] We include wavenumbers only up to $k_{\rm max} = 0.5h\,{\rm Mpc}^{-1}$ in the analysis, to avoid systematic uncertainties associated with non-linear clustering.

cluster sample detected with *CORE* via the thermal Sunyaev-Zel'dovich (SZ) effect [20] (see also Sec. 7); peculiar velocities as measured by the kinetic SZ effect [20]; and CMB lensing.

Lensing of the CMB *alone* is not a very powerful discriminant of models in which dark energy is only dynamically important at late times, since most, though not all, of the lensing effect in the CMB is sourced at too high a redshift. However, cross-correlation with tracers of large-scale structure at redshifts $z < 1$ isolates the lensing contribution during the period when dark energy is significant. As a probe of dark energy, CMB lensing from *CORE* will therefore be particularly powerful when combined with galaxy lensing and galaxy clustering data across redshift.

Combining *CORE* lensing with tomographic measurements of galaxy lensing adds a precisely determined high-redshift source plane and, as discussed above, allows cross-calibration of the majority of the expected galaxy lensing systematic effects. To illustrate these ideas, we consider constraints on dark energy models with equation of state parametrised in terms of the scale factor a as $w(a) = w_0 + w_a(1 - a)$, marginalising over the absolute neutrino mass and galaxy lensing systematic effects following Ref. [67]. We present results in terms of the dark energy figure of merit, FoM $= [\det \mathrm{cov}(w_0, w_a)]^{-1/2}$. With *Euclid* cosmic shear alone, the FoM is very dependent on whether or not poorly-understood non-linear scales are included in the analysis, degrading by an order of magnitude if the maximum wavenumber is reduced from $k_{\max} = 5.0h\,\mathrm{Mpc}^{-1}$ (FoM ≈ 50) to $1.5h\,\mathrm{Mpc}^{-1}$ (FoM ≈ 5). Combining with *CORE* data helps considerably, improving the FoM to approximately 300 using only linear scales from *Euclid*. These improvements will be significantly greater (FoM ≈ 2400) if strategies developed for internal calibration of *Euclid* data are successful (e.g., using image simulations to calibrate multiplicative bias in the estimation of galaxy shear). In this way, we can recover dark energy science from cosmic shear with *Euclid* using only relatively clean (quasi-)linear scales.

5.2 Galaxy clustering

Galaxies form preferentially within overdensities of the large-scale distribution of dark matter. Galaxy clustering is therefore potentially a powerful probe of the underlying mass distribution across cosmic time, and so of dark energy, modifications to gravity, neutrino masses, and the statistics of the primordial perturbations. Forthcoming galaxy redshift surveys (such as DESI, *Euclid*, and LSST) will extend significantly the statistical power of galaxy clustering measurements due to their large survey volumes, depths, and accuracy of redshifts.

A key issue in the interpretation of galaxy surveys is the uncertain relation between the clustering of galaxies and dark matter. On large scales, this is generally parameterised by a bias function $b(z)$, which depends on redshift as well as galaxy properties. Uncertainty in the bias limits the cosmological information that can be extracted from the broadband galaxy power spectrum. Lensing helps significantly in this regard since it probes the clustering of all mass along the line of sight back to the source. Lensing of background sources is correlated with the clustering of foreground galaxies, as the same large-scale structures that are traced by the foreground galaxies lens the background sources. By comparing the cross-correlation between the lensing of background sources and the galaxy overdensity (within some redshift range centred on z) with the auto-power spectrum of the galaxy overdensity, one can separate the bias $b(z)$ and clustering amplitude at that redshift with only weak model dependencies. For high-redshift galaxies, CMB lensing is particularly helpful as the last-scattering surface is so distant. This approach has recently been demonstrated with galaxies from DES [68] and, at higher redshift, from *Herschel* [69]. These tomographic analyses follow earlier work using

projected galaxy samples [9, 70–76]. With forthcoming galaxy clustering data, and high-S/N CMB lensing measurements over large fractions of the sky, this tomographic approach will allow precise tests of the growth of structure complementing other probes such as tomographic cosmic shear, redshift-space distortions, and the number counts of galaxy clusters.

5.3 High-redshift astrophysics

More generally, cross-correlating CMB lensing with other probes of large-scale structure has great promise as a probe of astrophysics at high redshift. A recent highlight of this approach is constraining the high-redshift star formation rate from correlations between CMB lensing and clustering of the cosmic infrared background (CIB) [77–81] – the unresolved flux from dusty, star-forming galaxies. In contrast to the CIB spectra across frequencies, the cross-correlation with lensing is insensitive to residual Galactic dust emission in the CIB maps, and does not require separation of the shot noise that arises from Poisson fluctuations in the number density of the galaxies that contribute to the CIB. A further application is constraints on gas physics in low-mass clusters and groups of galaxies, gas that is otherwise difficult to detect, from the correlation between CMB lensing and maps of the diffuse thermal SZ effect[7] [83]. Such measurements will be significantly advanced with the diffuse tSZ map from *CORE* [20], which should be much cleaner than the equivalent from *Planck* [84], and the improved S/N of the *CORE* lensing map. As a final application, we note the recent constraints on the bias and hence halo masses of high-redshift quasar hosts from cross-correlation of CMB lensing with quasar catalogues [73, 85]. With higher precision CMB lensing maps, such studies will be extended to probe dependencies on the quasar properties, such as redshift and luminosity.

6 Delensing B modes

One of the main science goals of *CORE* is to search for the distinctive signature of primordial gravitational waves in B-mode polarization [86, 87]. Primordial gravitational waves are a critical test of cosmic inflation in the early universe, and their detection would determine the energy scale at which inflation occurred and provide important clues to the physics of inflation. The inflationary science case for *CORE* is discussed in detail in Ref. [18].

Lensing of the CMB converts E-mode polarization into B-mode [24], and these lens-induced B-modes are a source of confusion in searches for primordial gravitational waves. However, it is possible partially to remove the lensing B-modes in a process known as "de-lensing"; essentially, this involves remapping the observed polarization with an estimate of the CMB lensing deflections [6–8]. In this section, we discuss the prospects for delensing with *CORE*.

The B-modes produced from conversion of E-mode polarization by lensing are approximately

$$B_{lm}^{\rm lens} = -i(-1)^m \sum_{LM} \sum_{l'm'} \begin{pmatrix} l & L & l' \\ -m & M & m' \end{pmatrix} {}_{-}F^2_{lLl'} \phi_{LM} E_{l'm'} \,, \tag{6.1}$$

where the geometric coupling term ${}_{-}F^2_{lLl'}$ is given in Appendix A. The power spectrum $C_l^{BB,{\rm lens}}$ is therefore

$$C_l^{BB,{\rm lens}} \approx \frac{1}{2l+1} \sum_{Ll'} \left({}_{-}F^2_{lLl'}\right)^2 C_L^{\phi\phi} C_{l'}^{EE} \,, \tag{6.2}$$

[7] The thermal SZ effect (e.g., Ref. [82]) is the Compton scattering of the CMB off hot ionized gas. Its characteristic frequency dependence allows separation from other emission components in multi-frequency maps.

and is shown in the left-hand panel of Fig. 3. For multipoles $l \lesssim 400$, $C_l^{BB,\rm lens} \approx 2.0 \times 10^{-6}\,\mu{\rm K}^2$ is almost constant, and so lens-induced B-modes act like an additional $5\,\mu$K arcmin of white noise on all scales relevant for detection of B-modes from primordial gravitational waves. This behaviour follows from the low-l limit of Eq. (6.2), which gives

$$C_l^{BB,\rm lens} \approx \frac{1}{2}\sum_{l'}\frac{2l'+1}{4\pi}l'^4 C_{l'}^{\phi\phi}C_{l'}^{EE}\,. \tag{6.3}$$

At multipoles $l > 10$, the B-mode lensing power spectrum exceeds that from primordial gravitational waves if the tensor-to-scalar ratio[8] $r \gtrsim 0.01$ (see Fig. 3). The best limits on r now come from B-mode polarization, with the combination of BICEP/Keck Array data and *Planck* and WMAP data (primarily to remove foreground emission from our Galaxy) giving $r < 0.09$ at 95 % C.L. [88]. Large-scale lensing B-modes are produced from E modes and lenses over a broad range of scales, with 50 % of the power at a multipole of 60 coming from lenses at multipoles $L > 400$. This is illustrated in Fig. 7, where we plot the fractional contribution to the lens-induced B-mode power at a multipole of 60 per multipole of the lensing potential, i.e., $d\ln C_{60}^{BB,\rm lens}/d\ln C_L^{\phi\phi}$. The generation of large-scale B-modes from E-modes and lenses on significantly smaller scales is the origin of the white-noise behaviour of $C_l^{BB,\rm lens}$.

The lensing B-mode power spectra can be accurately predicted in any model[9], with the uncertainty due to parameter errors at around the 0.5 % level for *CORE*. The main impact of lensing on the estimation of the primordial gravitational wave amplitude is therefore not from the average power that lensing contributes, subtraction of which causes only a small increase in parameter uncertainties, but rather the increased sample variance. We can illustrate the issue with the following crude approximation to the error on the tensor-to-scalar ratio estimated from the B-mode power spectrum:

$$\frac{1}{\sigma^2(r)} \sim f_{\rm sky}\sum_l \frac{2l+1}{2}\left(\frac{C_l^{BB,\rm gw}(r=1)}{rC_l^{BB,\rm gw}(r=1)+C_l^{BB,\rm lens}+N_l^{BB}}\right)^2\,, \tag{6.4}$$

where $C_l^{BB,\rm gw}(r=1)$ is the B-mode power spectrum from primordial gravitational waves for $r=1$ and N_l^{BB} is the power spectrum of the instrument noise. The presence of $C_l^{BB,\rm lens}$ on the right-hand side describes the effect of the sample variance of the lens-induced B-modes. This becomes important as noise levels approach $5\,\mu$K arcmin, and for an experiment such as *CORE* is the dominant source of "noise". Indeed, ground-based experiments have already reached this sensitivity for observations covering a few hundred square degrees (before foreground cleaning) [88].

The impact of lensing sample variance is shown in Fig. 8. The $3\,\sigma$ error on r is shown, based on Eq. (6.4), for three models: (i) $r=0$; (ii) $r = 4\times10^{-3}$, typical of the R^2 Starobinsky model [90] that predicts $r = 12/N_*^2$, where $N_* \approx 55$ is the number of e-folds between the end of inflation and the time that modes of wavenumber k_* exited the Hubble radius during inflation; and (iii) $r = 0.01$, roughly the forecasted detection limit of the current generation of

[8] The tensor-to-scalar ratio is the ratio of the primordial power spectra of gravitational waves and curvature fluctuations at a pivot scale k_*. Here, we adopt $k_* = 0.05\,{\rm Mpc}^{-1}$.

[9] Non-linear corrections to the matter power spectrum contribute to $C_l^{BB,\rm lens}$ at around the 6 % level on large scales [89]. The impact of systematic uncertainties in modelling the small-scale matter power spectrum, including the effects of baryonic physics, is a small change in the amplitude of $C_l^{BB,\rm lens}$ on large scales. This can be dealt with by marginalising over the amplitude of $C_l^{BB,\rm lens}$ during parameter estimation.

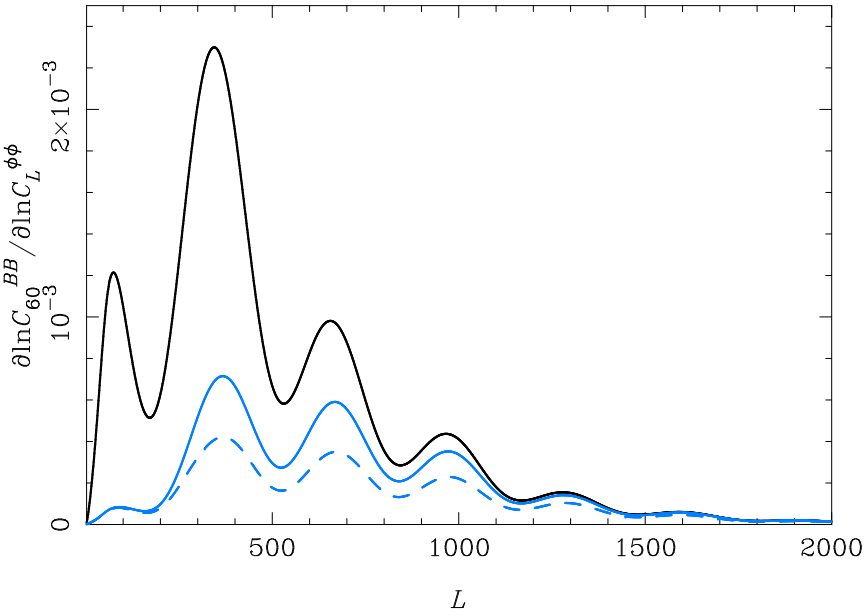

Figure 7. Fractional contribution to the lens-induced B-mode power at multipole $l = 60$ per multipole of the lensing potential. The black line shows the contribution before delensing, and so the area under the curve is unity. The impact of delensing is to suppress the contributions from lenses on scales where the S/N on the reconstructed lensing potential is high. This suppression is shown for internal delensing with *CORE* (solid blue), in which case the lensing power is reduced by 60 %, corresponding to a reduction in the error on r (for $r = 0$) by a factor 1.9. Combining with measurements of the CIB from *CORE* further helps suppress the smaller-scale lenses where the S/N on the reconstructed lensing potential is larger (blue dashed). In this case, the lensing power is reduced by 70 %, corresponding to a reduction in the error on r of 2.5.

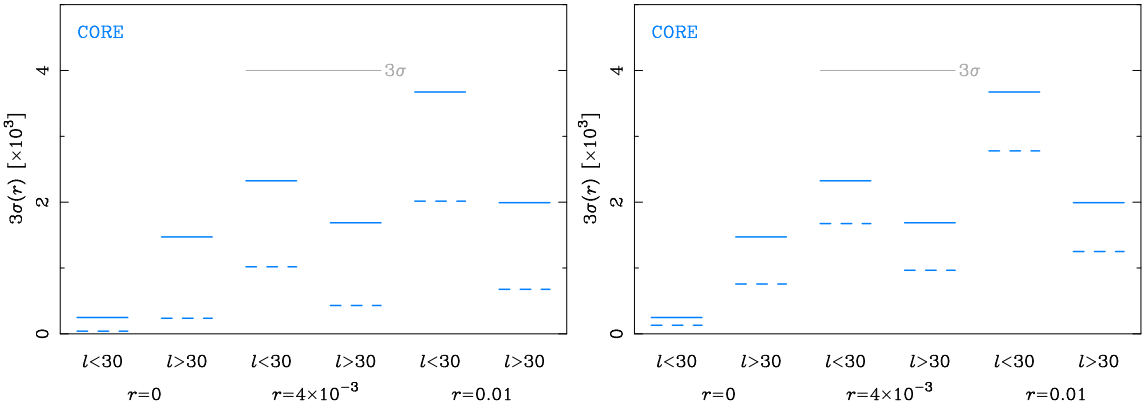

Figure 8. Impact of lensing on constraints on r from *CORE* for models with $r = 0$, $r = 4 \times 10^{-3}$ (typical for the Starobinsky model), and $r = 0.01$. For each model, the $3\,\sigma$ error (with all other parameters fixed) is shown using only BB for multipoles $l < 30$ (i.e., the signal from reionization) and $l > 30$ (the signal from recombination) over 70 % of the sky. The grey line shows the $3\,\sigma$ threshold for detecting $r = 4 \times 10^{-3}$. In the left-hand plot, the solid lines assume no delensing, while the dashed lines assume perfect delensing. In the right-hand plot, the solid lines again assume no delensing, but the dashed lines assume internal delensing. Effects of foreground removal are not included other than through our use of the weighted combination of the six 130–220 GHz channels for the effective instrument noise power.

sub-orbital experiments. Starobinsky inflation is an example of a model with a red spectrum of curvature fluctuations, with a tilt $n_s - 1 \propto -1/N_*$, which fits the measured temperature and E-mode polarization power spectra but produces a small $r \propto 1/N_*^2$. Such models will be natural targets for *CORE* if large-field models with $r \propto 1/N_*$ are ruled out by the time of flight. The errors on r are shown based on B-modes with $l < 30$ and $l > 30$. The former is intended to emphasise the constraints arising from the signal generated at reionization (see Fig. 3), while the latter isolates the signal from scattering around recombination. As discussed in Sec. 4, measuring the signals from reionization is likely only possible from space, but will be very important to confirm that any B-mode signal detected on degree scales is indeed due to primordial gravitational waves. We can draw the following conclusions from Fig. 8.

- In the limit that the signal sample variance is small compared to the lensing sample variance on all relevant scales, i.e., $rC_l^{BB,\rm gw}(r=1) \ll C_l^{BB,\rm lens}$, lensing increases the error on r by $1 + C_l^{BB,\rm lens}/N_l^{BB} \approx 6.5$ (for *CORE*) from both the reionization and recombination signals.

- For larger r, lensing has relatively more of an impact on the recombination signal than the reionization signal since $C_l^{BB,\rm gw}/C_l^{BB,\rm lens}$ is boosted at $l < 10$ by reionization.

- Lensing would limit the ability to test models such as Starobinsky inflation at very high significance on both reionization and recombination scales. For example, for $r = 4 \times 10^{-3}$, the sample variance of the lens-induced B-modes would limit the S/N with *CORE* to 7.1 from the recombination signal ($l > 30$), and $S/N = 5.1$ from the reionization signal at low multipoles. This situation is worsened for observations over smaller sky fractions.

To reduce the impact of sample variance of the lens-induced B-modes requires their coherent subtraction. Fortunately, such delensing is possible by combining the precise measurements of E-mode polarization from *CORE* with its lensing reconstruction. There are several ways to implement delensing, but for large-scale B-modes, where the gradient approximation of Eq. (6.1) is accurate, subtraction of a template constructed from the Wiener-filtered lens reconstruction and the Wiener-filtered E-mode polarization is close to optimal:

$$\hat{B}_{lm}^{\rm lens} = -i(-1)^m \sum_{LM} \sum_{l'm'} \begin{pmatrix} l & L & l' \\ -m & M & m' \end{pmatrix} {}_-F^2_{lLl'} \mathcal{W}_L^\phi \hat{\phi}_{LM} \mathcal{W}_{l'}^E E^{\rm dat}_{l'm'} \,. \tag{6.5}$$

Here, the Wiener filters are $\mathcal{W}_l^\phi = C_l^{\phi\phi}/(C_l^{\phi\phi} + N_l^{(0)})$ and $\mathcal{W}_l^E = C_l^{EE}/(C_l^{EE} + N_l^{EE})$, $\hat{\phi}$ is the lens reconstruction, and $E^{\rm dat}$ is the observed (noisy) E-mode polarization after deconvolution of the instrument beam. After subtracting the synthetic B-modes in Eq. (6.5) from the observed B-modes, the residual lensing power is approximately

$$C_l^{BB,\rm delens} \approx \frac{1}{2l+1} \sum_{Ll'} \left({}_-F^2_{lLl'}\right)^2 C_L^{\phi\phi} C_{l'}^{EE} \left(1 - \mathcal{W}_L^\phi \mathcal{W}_{l'}^E\right) . \tag{6.6}$$

In the limit that the S/N on the E-mode polarization is large on the scales relevant for lensing conversion to large-angle B-mode polarization, $\mathcal{W}_l^E \approx 1$. The contribution to the residual B-mode power from lenses at multipole L is therefore suppressed by a factor $1 - \mathcal{W}_L^\phi$, so that $\mathcal{W}_L^\phi$ gives the scale-dependent delensing efficiency. Figure 7 shows the contribution to the residual

B-mode power per lensing multipole as a fraction of the original lensing power at multipole $l = 60$, i.e., $(1 - \mathcal{W}_L^\phi) d\ln C_{60}^{BB,\rm lens}/d\ln C_L^{\phi\phi}$, for the minimum-variance lens reconstruction with *CORE*. The contribution is strongly suppressed for lenses on scales where the S/N on the reconstruction is high, making the delensed spectrum even closer to white noise on large scales than the spectrum before delensing. The integrated effect is a reduction of 60 % in $C_l^{BB,\rm lens}$ by internal delensing. The impact for constraints on r with *CORE* is illustrated in the right-hand plot in Fig. 8. Here, we have assumed that the residual B-modes after delensing are approximately Gaussian on large scales [as we also assumed in Eq. (6.4)]. For Starobinsky inflation, internal delensing improves the S/N on r to 12.5 from $l > 30$, allowing critical tests of this important class of models through detailed characterisation of the B-mode spectrum. For models with very low r, delensing improves $\sigma(r)$ by a factor of two on all scales. Internal delensing of B-modes (and the temperature and E-mode polarization) has recently been demonstrated with data from *Planck*, although the *Planck* reconstruction noise means that only around 7 % of the B-mode lensing power can currently be removed [91].

Internal lens reconstructions from the CMB are noisy on small scales that still contribute significantly to the large-angle B-mode power. The inclusion of other tracers of the lensing potential with better S/N on small scales can therefore further improve B-mode delensing. The cosmic infrared background (CIB) is a particularly promising tracer [92, 93], since it is highly correlated (around 80 %) with CMB lensing [78]. In principle, delensing with the CIB alone can remove around 60 % of the lensing B-mode power but this requires very accurate subtraction of Galactic dust emission (in total intensity) when estimating the CIB from multi-frequency data. CIB delensing has recently been demonstrated in practice, both for delensing temperature anisotropies [94] and B-mode polarization [95]. We can also optimally combine an internal lens reconstruction and the CIB (see Ref. [96] for a recent example with *Planck* maps). The high-frequency channels of *CORE* make it uniquely capable of separating the CIB from Galactic dust. On large scales, the optimal combination is dominated by the lens reconstruction, while the CIB dominates on smaller scales where the S/N on the lens reconstruction is poor. Note that on these small scales, any residual dust contamination in the estimated CIB is less significant and a high degree of correlation with lensing can be maintained. Generally, for N tracers, I_i, of the lensing potential, with (cross-)power spectra $C_l^{I_i I_j}$ amongst themselves and $C_l^{I_i\phi}$ with the lensing potential, the optimal combination for delensing is

$$\phi_{lm,\rm WF} = \sum_{ij} C_l^{I_i\phi} [\mathsf{C}_l^{-1}]_{ij} I_{lm,j}\,, \tag{6.7}$$

where the components of the matrix C_l are $C_l^{I_i I_j}$. Using $\phi_{lm,\rm WF}$ to construct the B-mode template (6.5), the residual power after delensing is still given by Eq. (6.6) but with $\mathcal{W}_l^\phi$ replaced with ρ_l^2, where ρ_l is the correlation coefficient between $\phi_{\rm WF}$ and ϕ with

$$\rho_l^2 = \frac{\sum_{ij} C_l^{I_i\phi} [\mathsf{C}_l^{-1}]_{ij} C_l^{I_j\phi}}{C_l^{\phi\phi}}\,. \tag{6.8}$$

We show the product $(1 - \rho_L^2) d\ln C_{60}^{BB,\rm lens}/d\ln C_L^{\phi\phi}$ in Fig. 7 for the combination of the minimum-variance lens reconstruction from *CORE* and the CIB at 500 GHz, using models from Ref. [78] for the CIB spectra. We assume negligible dust contamination and instrument noise in the CIB map. With this approach, we can remove 70 % of the lensing B-mode power on large angular scales (cf. 60 % without the CIB), which corresponds to an improvement in the tensor-to-scalar ratio (for $r = 0$) by a factor of 2.5 compared to no delensing.

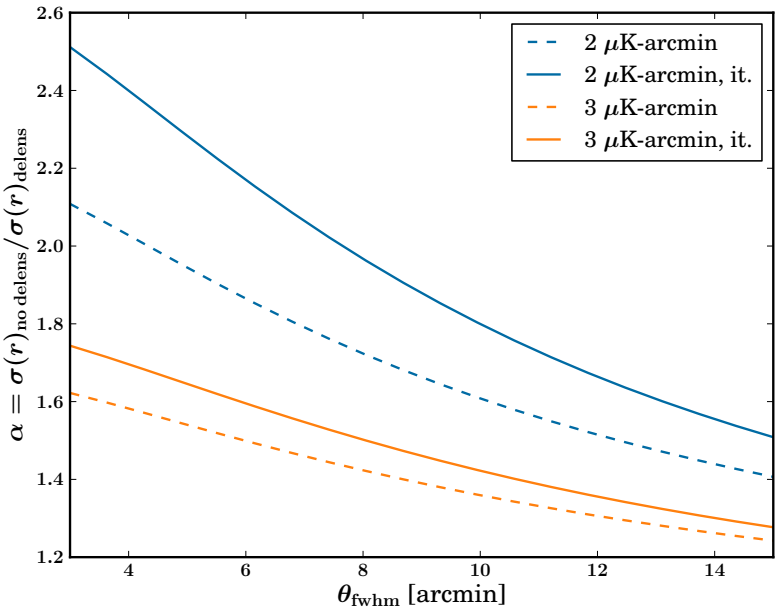

Figure 9. Fractional improvement in constraints on r, assuming $r = 0$, by internal delensing as a function of the angular resolution in the range relevant for space-based experiments. Results are shown for polarization noise levels of 3 μK arcmin (orange) and 2 μK arcmin (blue), without (dashed) and with (solid) iterative delensing.

Finally, we return to the issue of more optimal lens reconstruction that we discussed briefly in Sec. 2. There, it was noted that one can improve over reconstructions based on quadratic estimators for noise levels comparable to or better than the lensing B-mode noise (i.e., 5 μK arcmin). The noise levels on reconstructions that properly maximise the posterior distribution of ϕ given the observed CMB fields have been shown (in simulations; e.g., Ref. [37]) to be well reproduced by an approximate iterative calculation of the noise power $N_l^{(0)}$ of the quadratic estimator [39]. Here, we use the implementation described in Ref. [97], which uses only the EB estimator. Figure 9 shows the fractional improvement in $\sigma(r)$, for $r = 0$, from iterative delensing and the simple quadratic estimator compared to no delensing. The comparisons are made as a function of angular resolution and for two representative polarization noise levels. For the baseline specifications of *CORE* (effective beam size of 6.2 arcmin and 2.1 μK arcmin noise), the improvement in $\sigma(r)$ is around 1.9 for the quadratic estimator and 2.2 for iterative delensing.[10] For non-zero r, the relative gain in $\sigma(r)$ from iterative delensing would be smaller. More substantial gains are achieved at higher angular resolution and with lower noise, and so optimising delensing will be important for forthcoming deep ground-based surveys.

[10]The result for the quadratic estimator is a little worse than that quoted earlier, which was based on the minimum-variance quadratic estimator.

7 Cluster mass calibration

The abundance of galaxy clusters as a function of mass and redshift is a sensitive probe of the evolution of density fluctuations at late times. In particular, it is sensitive to the matter density parameter, $\Omega_{\rm m}$, the equation of state of dark energy, $w(a)$, and the amplitude of the fluctuations, σ_8. In recent years, large cluster samples have been assembled with clusters detected via the thermal Sunyaev-Zel'dovich (tSZ) effect in data from *Planck* [98], ACT [99], and SPT [100]. Compared to selection in other wavebands, the tSZ approach has a particularly well-understood selection function and can be extended to high redshifts. In its baseline configuration, *CORE* will detect around 40 000 clusters over the full sky ($S/N \geq 5$), significantly extending current catalogues. The combination of the many frequency channels of *CORE* and the deep, high-resolution imaging that is possible from the ground (e.g., with CMB-S4) is particularly powerful and could detect around 200 000 clusters [20]. The statistical power of such catalogues is very high, but in order to extract cosmological information from cluster abundances accurate estimates of cluster masses are needed. Cluster masses can be estimated via the cluster X-ray signal assuming hydrostatic equilibrium, an assumption that can be violated in several scenarios (e.g., bulk motions in the gas or nonthermal sources of pressure [101–103]). Alternatively, galaxy lensing offers another way to estimate cluster masses via the cluster-induced gravitational shear (see, e.g., Ref. [104] in the context of tSZ-selected samples). This approach is independent of the complex baryonic physics involved in X-ray estimates and directly probes the total mass. However, it is difficult to extend to high-redshift clusters due to the paucity of background sources and the uncertainty in source redshifts.

It has long been suggested that CMB lensing can be used to measure cluster masses [105]. In the absence of the cluster, the CMB is smooth on arcmin scales, and so cluster lensing induces a dipole-like signal aligned with the local background gradient of the temperature/polarization anisotropies. Initially, subtraction of this background gradient to measure directly the deflection field was suggested [106, 107], but this proved difficult. However, approaches based on the application of the quadratic estimators designed for lensing by large-scale structure, or on some modified version of them, have proved more satisfactory on simulated data [108–110]. Once the lensing deflections have been reconstructed, the cluster mass can be extracted optimally by application of a matched filter based on the expected cluster profile (e.g., an NFW profile [111]) [112]. Alternatively, cluster parameters can be estimated directly from the lensed CMB fields with a parametric maximum-likelihood approach [113]. Cluster mass estimation via CMB lensing is particularly promising for large samples of high-redshift clusters, where mass estimation by other means is very difficult.

Current high-resolution CMB observations are not sufficiently sensitive to allow measurement of individual cluster masses via CMB lensing. However, the mass scale of a cluster sample with a sufficiently large number of elements can be estimated with moderate S/N. Using data from SPT, the mass scale of 513 clusters was estimated via a parametric maximum-likelihood approach [114], yielding results consistent with the SZ-estimated mass scale and with the null hypothesis of no lensing rejected at $3.2\,\sigma$. For *Planck* clusters, the approach proposed in Ref. [112] was followed to estimate the hydrostatic bias parameter b that relates the X-ray derived mass M_X and the true mass M_{500}: $M_X = (1-b)M_{500}$ [98]. If the true mass is identified with a lensing-derived mass, galaxy lensing prefers a low value for $1-b$, somewhere in between 0.6 and 0.8, which significantly relaxes the tension between the observed cluster counts and those predicted in the ΛCDM model with parameters de-

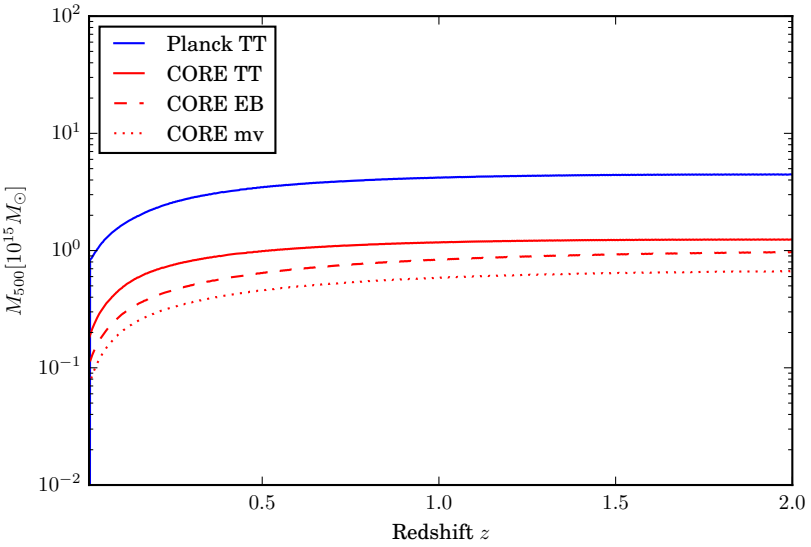

Figure 10. Limiting cluster mass as a function of redshift for which the S/N on a CMB lensing mass measurement with *CORE* is unity for an individual cluster. Results are shown for the TT (red solid), EB (red dashed), and minimum-variance (red dotted) quadratic estimators. For comparison, the equivalent for temperature reconstructions at the sensitivity of *Planck* is also shown.

termined from the primary CMB fluctuations. However, CMB lensing prefers a smaller bias (specifically, $1/(1-b) = 0.99 \pm 0.19$), which goes in the opposite direction of increasing the tension with the primary fluctuations.

The current applications of cluster lensing of the CMB only make use of temperature observations. Indeed, for the noise levels of an experiment like *Planck*, the TT quadratic estimator has the lowest reconstruction noise. However, for an experiment such as *CORE*, the EB estimator will be the most powerful, as in the case of lensing by large-scale structure (Sec. 2). This is significant since polarization-based measurements should remove several astrophysical sources of systematic error that complicate measurements based on temperature. These include residual tSZ emission, the kinetic SZ effect from cluster rotation (which induces a dipole-like signal with a CMB frequency spectrum), and residual infrared emission from galaxies within the cluster or along the line of sight.

The potential of cluster mass measurements with *CORE* is illustrated in Fig. 10, which shows, as a function of redshift, the minimum cluster mass with a mass measurement of $S/N = 1$. Here, lensing is reconstructed with quadratic estimators using multipoles $l \leq 3000$ in temperature and polarization, and the mass estimated using the matched-filter method described in Ref. [112]. The filter uses an NFW profile, truncated as $5r_{500}$ (where r_{500} is the radius at which the mass enclosed is 500 times that for a uniform density equal to the critical density at the cluster redshift). Results are shown for the TT, EB, and minimum-variance quadratic estimators. Similar results for TT only can be found in Ref. [20].[11] We use noise levels for the combination of CMB channels used throughout this paper, assuming that

[11]The TT results there are not directly comparable with those in Fig. 10 due to several differences in implementation, including the maximum multipole used in the analysis.

this is representative of the noise after astrophysical foreground removal. We additionally propagate the effects of lensing by large-scale structure (assumed independent of the cluster lensing) to the forecasted errors on our mass measurements. For comparison with previous experiments, results are also shown for a *Planck*-like experiment with temperature noise levels of 45 μK arcmin and a Gaussian beam with FWHM of 5 arcmin. Figure 10 shows that the EB estimator is more powerful than TT for *CORE*, and that the improvement with respect to *Planck* is significant. Individual cluster masses can be measured with $S/N \geq 1$ for all clusters with $M_{500} > 10^{15}\,M_{\odot}$ irrespective of redshift and over the full sky; the accuracy is considerably better than this below $z = 0.5$. While *CORE* lacks the resolution to be able to measure individual masses for typical clusters that it will detect, the large sample size means that scaling relations between tSZ observables and the true mass can be accurately calibrated [20]. For example, assuming that the hydrostatic bias parameter b is independent of mass and redshift, *CORE* will be able to calibrate this at the percent level using the clean EB estimator.

8 Impact of Galactic foregrounds on lensing reconstruction

Polarized emission from Galactic dust is now known to be a major issue for attempts to detect B-modes from primordial gravitational waves [115, 116]. Any internal reconstruction of the CMB lensing potential will also be contaminated by residual foregrounds in the observed region of the sky. Since lensing estimators rely on extracting the non-Gaussian signature in the observed CMB that is characteristic of gravitational lensing (see Sec. 2), inherently non-Gaussian foreground fields such as Galactic dust are of particular concern for lensing studies [117]. Given that the EB quadratic estimator will provide most of the lensing information for *CORE*, characterising the contamination of polarized dust emission to the recovered lensing power spectrum is of vital importance. While most of the S/N on lens reconstructions at multipole L from TT and EE come from squeezed shapes, i.e., CMB modes at multipoles $l \gg L$, this is not true for the more powerful EB reconstruction except on the largest scales; a significant fraction of the S/N comes from B-modes with $l < 1000$ for any L [118]. As the dust B-mode power spectrum is much redder than the B-mode spectrum from lensing, one might expect dust to be a significant contaminant for EB reconstructions at all multipoles L. Indeed, *Planck* 353 GHz data show that over 70 % of the sky, the expected dust B-mode power at 150 GHz exceeds the lensed B-mode power at all multipoles [115].

For intermediate and high Galactic latitudes, the large-scale ($40 < l < 600$) angular power spectra of the dust polarization are well constrained by *Planck* observations at 353 GHz, which are dominated by polarized Galactic dust emission [115]. For observations away from the Galactic plane, the dust power spectra at 353 GHz are well-modelled by a single power law $C_l^{XX} = A_{\rm dust}^{XX}(l/80)^{\alpha}$ for $X \in \{E, B\}$ and $\alpha = -2.42 \pm 0.02$. Dust polarization arises from the alignment of aspherical grains in the Galactic magnetic field (e.g., Refs. [119–121]). In Ref. [122], Gaussian simulations of the turbulent magnetic field in the Galaxy are used to argue that the power-law slope α of the polarization angular power spectra directly reflects the slope of the power spectrum of the turbulent field. The polarized dust power-spectral amplitude $A_{\rm dust}^{EE}$ (given in $\mu{\rm K}^2_{\rm CMB}$ at 353 GHz) varies significantly with sky coverage: $A_{\rm dust}^{EE} = 37.5 \pm 1.6$ for the cleanest 24 % of the sky, while $A_{\rm dust}^{EE} = 328.0 \pm 2.8$ for the cleanest 72 %, reflecting the large variation in dust column density across the sky. The amplitudes $A_{\rm dust}^{BB}$ are approximately half the corresponding $A_{\rm dust}^{EE}$ amplitudes.

A Gaussian and statistically-isotropic dust contribution would add noise to the lensing reconstruction, but could be handled straightforwardly and optimally using existing filtering techniques. Note that such filtering requires knowledge only of the total power spectra (including CMB, foregrounds and noise), which can be approximated by smoothed versions of the measured spectra, and fiducial lensed CMB power spectra. Such Gaussian and statistically-isotropic dust would propagate no bias into the lensing power spectrum or derived parameters. The statistical anisotropy of dust can also be handled with existing techniques if reconstructions are made locally. Using a realisation-dependent calculation of the Gaussian noise-bias $N_L^{(0)}$ would mitigate against small errors in simulating the dust locally as being statistically isotropic, with power spectra calibrated within each patch [123]. Rather, it is the non-Gaussianity of dust emission that is particularly problematic for lensing studies. The alignment of dust grains, which sources the polarized emission, and their spatial distribution are highly complex and imperfectly modelled. There is large variation in the Galactic magnetic field orientation along any given line of sight, and this leads to scatter in the polarization fraction [124]. The trispectrum of the dust emission will bias estimates of the lensing power spectrum, with the bias going like the fourth power of the polarized dust amplitude.

One hindrance to quantifying the dust bias to lensing is that the small-scale polarization field of the dust is not well constrained by current data. For future surveys, the extent of the dust contamination of lensing estimators is therefore not well known; there is considerable model uncertainty about the expected amplitude and shape of the dust four-point signal. Here, we consider dust maps constructed for the *Planck* FFP8 simulations [125]. While these are well motivated in that they are data-derived (principally from *Planck* 353 GHz observations), the polarization observations in particular are extremely noisy at small scales.[12] These tracer maps therefore cannot be fully representative of the small-scale dust polarization on the sky that will be seen by *CORE*. Another approach under investigation is to derive a dust polarization tracer map from observations of Galactic neutral hydrogen (HI), for which the filamentary structure has been shown to correlate strongly with the orientation of the Galactic magnetic field, and hence the dust polarization angle [124, 126]. Whether these different dust tracers yield similar inferences about the lensing dust bias is the subject of ongoing work. As a space-based CMB experiment, *CORE* will allow for precision observations at high frequencies – something that is unattainable from the ground, and therefore an obvious concern for ground-based experiments such as CMB-S4. *CORE* observations would thereby eliminate the data deficiency on the small-scale dust polarization, allowing for a direct measurement of dust bias and, more practically, providing the high-frequency data needed for dust subtraction through component-separation techniques (see Ref. [127] for a detailed analysis of component separation for *CORE*).

Given that the dust power spectra fall rapidly with multipole, one way to reduce dust contamination is to exclude large-scale modes from the lensing reconstruction analysis [117]. In the choice of the minimum multipole $l_{\rm min}$ to use in the analysis, there is a trade-off between bias and variance: including more modes will reduce the sample variance, but the filtered

[12]The construction of the simulated maps is described in detail in Ref. [125]. The degree and orientation of dust polarization on scales larger than 0.5 deg are derived from the ratio of smoothed maps of the Stokes parameters Q and U at 353 GHz and the GNILC-reconstructed map of the dust total intensity. These ratio maps are extended to smaller scales with a Gaussian realisation. Finally, the full-resolution polarization maps are obtained by multiplying with the total intensity GNILC dust template. The small-scale dust polarization inherits non-Gaussianity from the total intensity, but does not properly reflect the non-Gaussian structure due to the small-scale Galactic magnetic field.

maps will be correspondingly contaminated by non-Gaussian large-scale dust modes that will propagate into a lensing bias. As discussed above, the strong spatial variation of the dust signal may suggest performing reconstructions locally. The choice of the minimum multipole $l_{\rm min}$ to use in the analysis may vary depending on the position of observed patch relative to the Galaxy. Furthermore, the lensing signal is extracted through weighted combinations of filtered versions of the observed fields, with the optimal filters themselves dependent on the local dust power spectrum, again suggesting a local approach to lensing reconstruction.

As well as signals from our Galaxy, non-Gaussian extragalactic foregrounds can bias lens reconstruction. Potential biases for the TT quadratic estimator are studied in Ref. [38]. For temperature observations, bright galaxies (flux density $F_{150\,\rm GHz} \gtrsim 1\,$mJy) and massive galaxy clusters ($M \gtrsim 10^{14} M_\odot$) must be appropriately masked, and a maximum multipole $l_{\rm max} \approx 2500$ used for lensing reconstruction, to reduce the induced bias to acceptable levels for *CORE*. The extra-Galactic contamination in polarization is not robustly quantified, but is expected to be less problematic due to the typically low polarization fraction of these sources [39].

8.1 Quantifying lensing bias from Galactic dust

The broad frequency coverage of *CORE* will allow for accurate foreground subtraction through component separation techniques [127] and a corresponding mitigation of the lensing bias. Here, we attempt to bound the overall bias to the lensing potential power spectrum by performing lensing reconstruction on CMB simulations over a field of $600\,{\rm deg}^2$, to which a fixed realisation of bright dust emission is added in temperature and polarization, with no component separation performed. The field chosen has the brightest dust emission of all regions of this size that lie outside the *Planck* analysis mask, and so likely will be included in the *CORE* lensing analysis; the results therefore represent a rough upper bound on the dust contamination. The dust tracer map is more reliable in regions of bright emission because of the lower fractional contamination from residual CIB or detector noise. The dust intensity at 150 GHz in this field is shown in Fig. 11 along with its corresponding 1-point distribution. For comparison, we also show the 1-point function of dust intensity emission of the cleanest $600\,{\rm deg}^2$ region, near the Southern Galactic pole, in which the root-mean-square intensity fluctuations are an order-of-magnitude below our analysis field.

The bias to the lensing reconstruction from dust emission is quantified as follows. Appropriately-correlated Gaussian CMB realisations on the flat sky are drawn from fiducial spectra based on the *Planck* best-fit cosmological parameters [115]. The temperature and polarization fields are lensed by remapping with the gradient of a Gaussian lensing potential, itself drawn from the fiducial lensing potential power spectrum. The fixed dust realisation and scale-dependent Gaussian noise appropriate for the *CORE* CMB channels[13] are added to these lensed simulations. The lensing potential is then reconstructed using flat-sky implementations of the quadratic estimators [32] from the `quicklens` package.[14] When filtering the CMB fields, $X \to \bar{X}$ [see Eq. (2.2)], during lens reconstruction, we include a model dust power spectrum, obtained as a power-law fit to the dust power spectra in this particular region on the sky. Failure to include the dust power in the filtering can lead to

[13] The noise level is determined from the combination of *CORE*'s CMB channels, i.e., the six channels in the range 130–220 GHz, used for forecasts throughout this paper. The assumed dust level in the field has not been corrected for (weighted) averaging the dust spectral energy distribution across these channels; rather it is simply the emission at 150 GHz.

[14] https://github.com/dhanson/quicklens

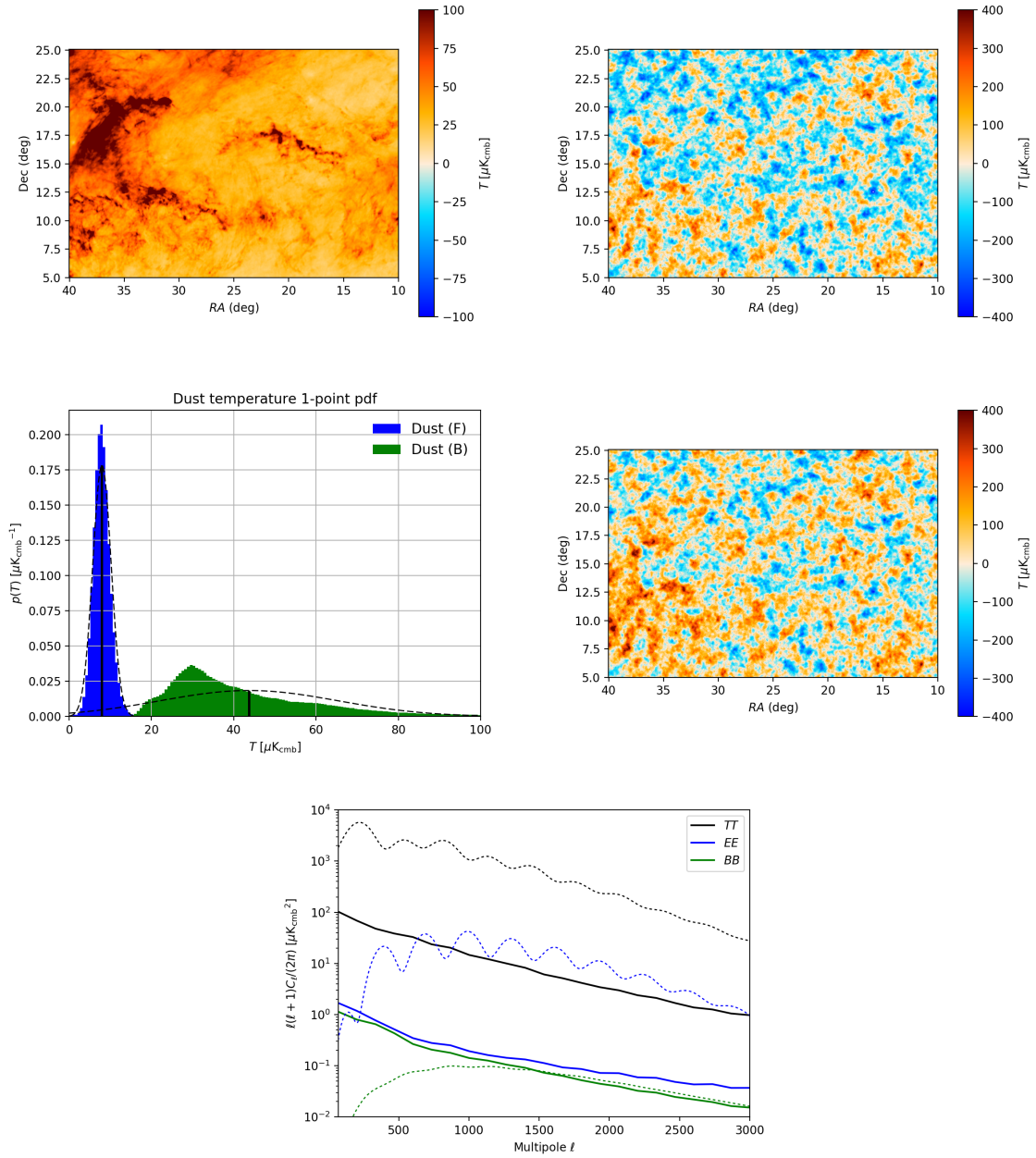

Figure 11. *Top left*: Dust emission in total intensity at 150 GHz in the analysis field. The diffuse, non-Gaussian nature of the dust emission is clear. For comparison, the r.m.s. CMB fluctuations are around 70 μK. *Middle left*: Pixel histogram (1-point function) for the dust intensity. The field used in this analysis is labelled 'B' and coloured green; the non-Gaussianity of the 1-point density is apparent when compared against the black-dashed Gaussian distribution that has the same mean and dispersion. The field labelled 'F' and coloured blue comes from the cleanest 600 deg^2 patch of dust emission near the Southern Galactic pole. The CMB temperature (*Planck* `SMICA` map) in the analysis region is also shown without (*top right*) and with (*middle right*) the additive dust emission component; the effect of dust at 150 GHz is visible by eye in this region. *Bottom*: Dust power spectra in the analysis patch (solid lines). CMB fluctuations (dashed lines) dominate the variance in temperature, but in polarization the BB dust power spectrum is greater than or comparable to the CMB spectrum for all scales, while the EE dust spectrum exceeds the CMB spectrum on large scales.

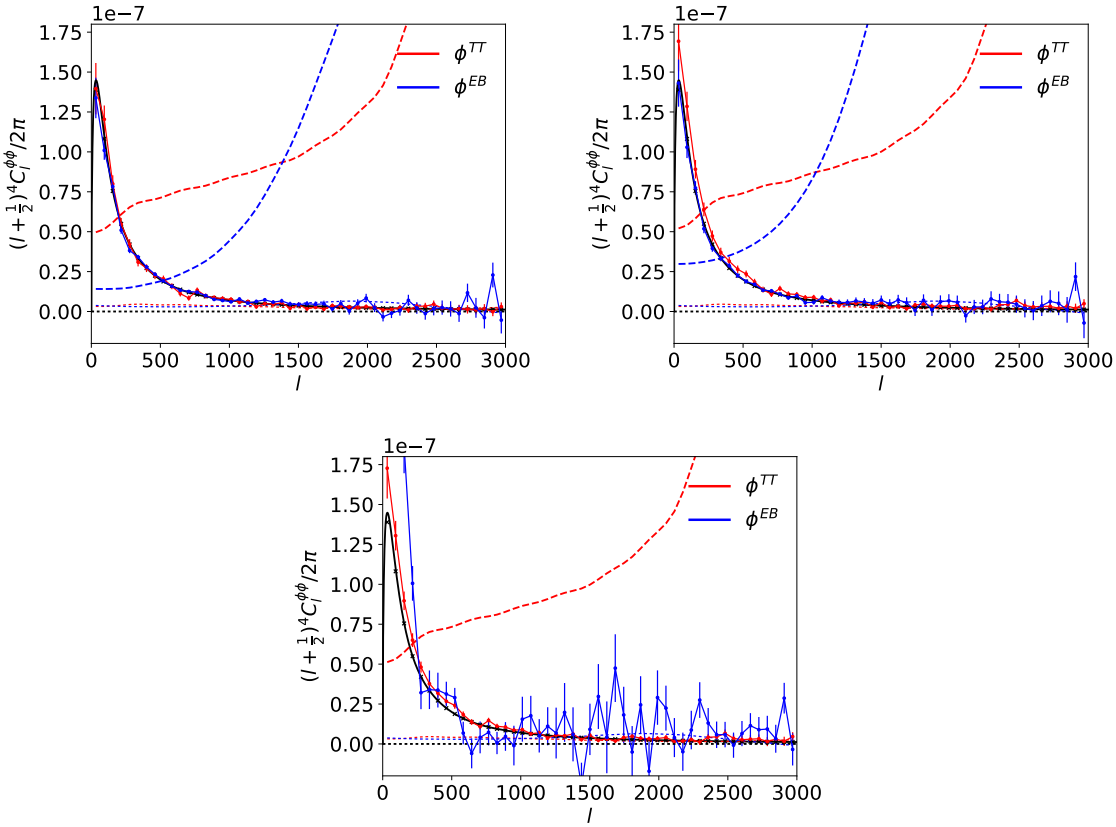

Figure 12. *Top left*: Mean lensing power spectrum reconstructions over five mock *CORE* observations at 150 GHz, including realistic noise, with no dust contamination. The lensing power spectrum (black solid line) is recovered in an unbiased fashion (see also Table 1). Dashed lines show the $N_L^{(0)}$ Gaussian noise power in the reconstructions, and dotted lines are the small $N_L^{(1)}$ biases. The measured spectra are corrected for both such biases. The lensing detection significance of the EB reconstruction has about twice the power of TT in the no-dust case. *Top right*: As top left, but with the dust field added before reconstruction, and including the dust power in the lensing filters. The bias from dust is clear by eye in the temperature reconstruction (red points). With this filtering for *CORE*, we expect a roughly 15 % bias for the TT estimator and negligible bias for EB. Note that these results are specific to this bright dust field, and assume no Galactic foreground removal. It can be seen that uncertainties are inflated relative to the no-dust case due to the additional variance of the dust component. *Bottom*: As top right, but without including the dust power in the filtering. In this case the EB reconstruction is highly sub-optimal (the $N_L^{(0)}$ Gaussian noise power is off the scale of the plot) and biased. There is little change in the TT reconstruction as the dust power is subdominant to the CMB power. In all panels, the error bars are analytic estimates from $N_L^{(0)}$ and $C_L^{\phi\phi}$ and have been scaled to reflect $f_{\rm sky} = 0.7$. The same CMB and noise realisations are used in all panels.

biased and sub-optimal reconstructions (see Table 1). The minimum CMB multipole used is $l_{\rm min} = 12$ corresponding to the longest non-constant mode supported on the patch. The mean auto-power spectra of the TT and EB reconstructions are shown in Fig. 12. The realisation-dependent $N_L^{(0)}$ bias and an analytic approximation of the sub-dominant $N_L^{(1)}$ bias have been subtracted from the raw power spectrum to obtain an unbiased estimator (in the absence of non-Gaussian foregrounds) of the underlying lensing power.

	No dust	Bright dust field	Bright dust field (inc. dust power in filters)
$TT \times TT$	$A = 1.002 \pm 0.008$	$A = 1.169 \pm 0.008$	$A = 1.158 \pm 0.008$
$EB \times EB$	$A = 0.997 \pm 0.004$	$A = 1.615 \pm 0.030$	$A = 0.999 \pm 0.006$

Table 1. Fits to the lensing power spectrum amplitude A for mock *CORE* observations at 150 GHz (see Fig. 12). Fits are performed over the multipole range $2 \leq L < 3000$ for the recovered lensing power spectrum from the TT and EB estimator. The central value quoted is the mean over five simulations, while the error is appropriate to a single realisation and has been scaled to reflect a full-sky analysis ($f_{\rm sky} = 0.7$). The standard error on the mean of A is a factor 3.1 larger than the errors shown. We see that without dust the input amplitude can be recovered to high accuracy. Performing the reconstruction over a dusty region induces bias in both estimators and additional variance for EB. When including the dust power in the lensing filters, the bias in the power from the EB estimator is removed, but a 15 % bias remains for the TT estimator since including the dust power makes only a small change to the temperature filter on the (small) scales that dominate the TT reconstruction. Note that no foreground removal is assumed in this analysis.

We note that here we scale the 353 GHz dust emission to an effective 150 GHz observing channel using a modified black body spectrum with temperature $T_{\rm dust} = 21$ K and spectral index $\beta_{\rm dust} = 1.5$. We add this scaled dust component to noisy, lensed CMB maps with noise level appropriate to the combination of *CORE*'s CMB channels, i.e., the six channels in the range 130–220 GHz, used for forecasts throughout this paper. This procedure is more akin to how a ground-based experiment with sensitivity around 2 μK arcmin at 150 GHz would observe and analyse the CMB sky. Since dust emission rises strongly with frequency, the actual level of dust emission in the six-channel combination, based on inverse-noise-variance weighting, would be around a factor of 1.5 higher than at 150 GHz assuming no component separation.

We distill the effect of the dust bias by fitting a lensing amplitude parameter A, which scales the amplitude of the fiducial lensing power spectrum, to the estimated power spectrum. Any statistically-significant deviation from unity in this parameter ($A \neq 1$) represents biasing from the dust emission which, if unmodelled, would directly impact any cosmological inference from the lensing measurement. For example, the effect of neutrino mass is to suppress the lensing power spectrum (Sec. 5); a bias in the lensing amplitude A would therefore directly propagate into crucial cosmological parameters. To keep the bias well below the statistical error on a measurement of the lensing amplitude, we require biases below $O(0.1)$ % for an EB-based analysis.

The principal results of this analysis are shown in Table 1. For this region of the sky, with its atypically bright dust emission, the bias to *CORE* observations is around 15 % in the temperature reconstruction, but much smaller for EB (below the approximately 2 % level to which we have sensitivity with only the five simulations used here). This clarifies the need for *CORE* to perform lensing reconstruction on foreground-subtracted temperature maps. The addition of dust has little effect on the lensing detection significance for the TT estimator since the dust power is small compared to the CMB power. For the same reason, including dust power in the lensing filters is ineffective in mitigating the dust bias for temperature reconstructions. In this case, explicit high-pass filtering of the data may be more effective. In contrast, the dust power is comparable to, or larger than, the CMB polarization power across a wide range of scales, and therefore has a stronger effect on the lensing reconstruction

	No dust	Bright dust	50 % dust	20 % dust	10 % dust	1 % dust
$TT \times TT$	1.002 ± 0.008	1.169 ± 0.008	1.025 ± 0.008	1.007 ± 0.008	1.004 ± 0.008	1.002 ± 0.008
$EB \times EB$	0.997 ± 0.004	1.615 ± 0.030	1.004 ± 0.010	0.982 ± 0.005	0.994 ± 0.004	0.998 ± 0.004

Table 2. Fits to the lensing amplitude A for mock *CORE* observations over the bright dust field, as in Table 1, with the amplitude of the (residual) dust emission reduced down to the indicated percentage of the raw emission at 150 GHz. The dust power is not included in the lensing filters here, reflecting a global analysis.

uncertainties. These numerical conclusions were derived assuming that the model dust maps used are representative of the true dust emission on the sky; the present paucity of data on high-resolution dust polarization limits the scope to remove this caveat in the near future.

We also investigate how the lensing bias from dust is mitigated by reducing the amplitude of the dust emission by hand in the simulations. This process can be regarded as modelling the dust residuals after foreground cleaning, with the residual amplitude in the cleaned map expressed as a fraction of the dust emission at 150 GHz. We consider various levels of residual dust contamination (Table 2), and here do not include any dust power in the lensing filters, reflecting a global analysis. We see that, even in this particularly bright field, the dust bias can be reduced to acceptable levels for *CORE* (in both temperature and polarization reconstructions) if foreground cleaning can reduce the residual dust contamination to around 10 % of the amplitude of the raw emission at 150 GHz (1 % in power).

CORE will characterise the Galactic dust accurately – both in its spatial variation and in its spectral energy distribution – through its high-sensitivity, multi-frequency coverage and its high resolution in the dust-dominated channels. With component separation techniques this will allow for the construction of foreground-subtracted maps [127] on which lensing reconstruction can be performed, mitigating the dust bias. Ongoing work aims to quantify the residual lensing bias after foreground cleaning, accounting for the *CORE* specification of frequency channels and map-level sensitivities.

9 Conclusions

Weak gravitational lensing of the CMB has great potential as a relatively clean probe of the large-scale clustering of all mass to high redshift. *CORE* has been designed so that it is able to exploit much of this potential. We discussed how the lensing map reconstructed from *CORE* data would have statistical power significantly extending what can be achieved with the current generation of experiments. Lensing impacts many of the science goals of *CORE*; here we have highlighted its role in measuring the absolute neutrino mass scale, the growth of structure across cosmic time through cross-correlation with other large-scale structure surveys, delensing B-modes in searches for the polarization signal of primordial gravitational waves, and calibration of cluster masses for accurate interpretation of counts of galaxy clusters across redshift.

Current CMB lensing reconstructions are dominated by the temperature anisotropies. However, the lensing information that can be extracted from the temperature is severely limited by its Gaussian fluctuations, which add an irreducible noise to the reconstruction. Since B-mode polarization on intermediate and small scales is only expected to be produced by gravitational lensing, polarization-based reconstructions can circumvent this limitation. Moreover, while the interpretation of temperature-based reconstructions needs to take care-

ful account of non-Gaussian extragalactic foregrounds, polarization-based reconstructions are expected to be much cleaner. However, achieving a precise lens reconstruction with polarization requires sufficient sensitivity and resolution to image the faint lens-induced B-modes over a broad range of scales. One of the main science goals of *CORE* – searching for the B-mode polarization from primordial gravitational waves down to tensor-to-scalar ratios $r \sim O(10^{-3})$ [18] – already demands noise levels below the lens-induced B-modes on degree scales. By combining this sensitivity with angular resolution of around 6 arcmin, *CORE* is able to reconstruct lensing via the EB estimator over the full sky with S/N greater than unity *per mode* for lens multipoles $L < 500$. *CORE* is therefore uniquely able, amongst currently-proposed satellites, to delens its measured degree-scale B modes with an internal lens reconstruction. Generally, delensing requires a high-S/N proxy for the CMB lensing potential and high-S/N E-mode measurements both over a broad range of scales. We showed that *CORE* would be able to reduce the power of lens-induced B-modes by around 60 % with internal delensing. A similar level of delensing should be possible with the clean measurement of the cosmic infrared background from the multi-frequency *CORE* data, providing a valuable cross-check on results with internal delensing. CIB delensing is particularly helpful for small-scale lenses where the statistical noise on lens reconstructions becomes large. Indeed, the optimal combination of an internal lens reconstruction and the CIB can reduce the lensing B-mode power to around 70 %. In the null hypothesis, $r = 0$, this would improve the error on the tensor-to-scalar ratio by a factor 2.5 compared to no delensing.

Similar lensing performance to *CORE* could also be achieved with a future ground-based survey, e.g., CMB-S4 [33]. Improved angular resolution relaxes the noise requirement a little, but for similar statistical power one still needs polarization sensitivity better than 3 μK arcmin (at 1 arcmin resolution, for example) over nearly the full sky. To reach this sensitivity below the atmosphere requires roughly two orders of magnitude more detectors than on *CORE*. For the goal of measuring neutrino masses with CMB lensing, a critical limitation arises from uncertainty in the optical depth to reionization, τ. It is currently unknown, however, whether it will be possible to measure this parameter precisely with large-angle E-mode measurements from sub-orbital experiments. We infer the neutrino mass by its impact on the growth of structure from high redshift, as measured with the primary CMB fluctuations, to lower redshifts, as measured by CMB lensing. Our knowledge of the amplitude of the primordial fluctuations, $A_{\rm s}$, from the primary CMB is limited by uncertainty in the optical depth since only the combination $A_{\rm s}e^{-2\tau}$ is well determined. With lensing measurements of the precision expected from *CORE*, the total neutrino mass can be measured to a precision of 17 meV, when combined with contemporaneous BAO distance measurements, *provided that the optical depth is also measured to cosmic-variance limits.* This compares to the minimal mass implied by neutrino oscillations of approximately 60 meV. *CORE* is designed so that it can make precision measurements of the reionization feature in large-angle polarization and so determine τ to the cosmic-variance limit $\sigma(\tau) \approx 0.002$. In contrast, if we had to rely on the current *Planck* determination, with $\sigma(\tau) \approx 0.009$ [49], the error on the total neutrino mass would almost double to 30 meV and a detection would not be guaranteed.

Finally, we note that *CORE* is designed with broad frequency coverage so that it can accurately separate the CMB from Galactic and most extragalactic foreground emission [127]. We know from current attempts to measure degree-scale B-modes that accurate removal of Galactic dust is critical, even in the cleanest parts of the sky [116]. Lensing reconstruction mostly relies on smaller-scale modes of the CMB so the expectation is that foreground cleaning will be less demanding than for degree-scale B modes. We have attempted to quantify

this, presenting some preliminary results on the level of bias that would arise from (non-Gaussian) residual Galactic dust contamination in lensing power spectrum measurements. Even in the regions of brightest emission away from the Galactic plane, cleaning that suppresses the dust emission amplitude to 10 % of the raw emission at 150 GHz is sufficient to reduce the bias to acceptable levels. Cleaning to such levels should be achievable with *CORE*, and, of course, the demands are less stringent in regions with more typical levels of emission.

A Quadratic lensing reconstruction

The linear response of the covariance between lensed CMB fields $\tilde{X}_{lm}$ and $\tilde{Y}_{lm}$, where X and $Y = T$, E, or B, to a variation in the lensing potential is

$$\langle \delta(\tilde{X}_{l_1 m_1} \tilde{Y}_{l_2 m_2}) \rangle \approx \sum_{LM} (-1)^M \begin{pmatrix} l_1 & l_2 & l_3 \\ m_1 & m_2 & -M \end{pmatrix} \mathcal{W}^{XY}_{l_1 l_2 L} \delta\phi_{LM} \,. \tag{A.1}$$

The response functions are

$$\mathcal{W}^{TT}_{l_1 l_2 L} = C^{TT}_{l_2} {}_+F^0_{l_1 L l_2} + C^{TT}_{l_1} {}_+F^0_{l_2 L l_1} \,, \tag{A.2}$$
$$\mathcal{W}^{EE}_{l_1 l_2 L} = C^{EE}_{l_2} {}_+F^2_{l_1 L l_2} + C^{EE}_{l_1} {}_+F^2_{l_2 L l_1} \,, \tag{A.3}$$
$$\mathcal{W}^{TE}_{l_1 l_2 L} = C^{TE}_{l_2} {}_+F^0_{l_1 L l_2} + C^{TE}_{l_1} {}_+F^2_{l_2 L l_1} \,, \tag{A.4}$$
$$\mathcal{W}^{TB}_{l_1 l_2 L} = i C^{TE}_{l_1} {}_-F^2_{l_2 L l_1} \,, \tag{A.5}$$
$$\mathcal{W}^{EB}_{l_1 l_2 L} = i C^{EE}_{l_1} {}_-F^2_{l_2 L l_1} \,, \tag{A.6}$$

where C^{XY}_l are the lensed spectra, and we have defined

$$\begin{aligned} {}_\pm F^s_{l_1 L l_2} = \frac{1}{2} \left(1 \pm (-1)^{l_1+l_2+L}\right) & \left[L(L+1) - l_1(l_1+1) + l_2(l_2+1)\right] \\ & \times \sqrt{\frac{(2L+1)(2l_1+1)(2l_2+1)}{16\pi}} \begin{pmatrix} l_1 & L & l_2 \\ s & 0 & -s \end{pmatrix} . \end{aligned} \tag{A.7}$$

Note that the ${}_+F$ vanish for $l_1 + l_2 + L$ odd, and the ${}_-F$ for $l_1 + l_2 + L$ even. The response function $\mathcal{W}^{XY}_{l_1 l_2 L}$ are non-zero only for $l_1 + l_2 + L$ even for parity-even combinations, such as TT or TE, while they are non-zero only for $l_1 + l_2 + L$ odd for parity-odd combinations, such as TB and EB. Moreover, they are real for parity-even combinations and imaginary for odd parity, and satisfy $\mathcal{W}^{XY}_{l_1 l_2 L} = (-1)^{l_1+l_2+L} \mathcal{W}^{YX}_{l_2 l_1 L}$.

The optimal quadratic estimator was given in Eq. (2.2), which we repeat here for convenience:

$$\hat{\phi}^{XY}_{LM} = \frac{(-1)^M}{2} \frac{1}{\mathcal{R}^{XY}_L} \sum_{l_1 m_1, l_2 m_2} \begin{pmatrix} l_1 & l_2 & L \\ m_1 & m_2 & -M \end{pmatrix} [\mathcal{W}^{XY}_{l_1 l_2 L}]^* \bar{X}_{l_1 m_1} \bar{Y}_{l_2 m_2} \,. \tag{A.8}$$

Throughout this paper, we assume that the temperature and polarization fields are filtered independently, following Ref. [4]. In this case, for an isotropic survey the inverse-variance-filtered fields $\bar{X}_{lm} = F^X_l X_{lm}$, where the filter is the inverse of the total power spectrum: $F^X_l = 1/C^{XX}_{l,\mathrm{tot}}$. In this case, the normalisations of the quadratic estimators are

$$\mathcal{R}^{XY}_L = \frac{1}{2(2L+1)} \sum_{l_1 l_2} F^X_{l_1} F^Y_{l_2} |\mathcal{W}^{XY}_{l_1 l_2 L}|^2 \,. \tag{A.9}$$

Denoting an unnormalised estimator by an overbar, $\bar{\phi}^{XY}_{LM} = \mathcal{R}^{XY}_L \hat{\phi}^{XY}_{LM}$, the disconnected contribution to its power spectrum is $\langle \bar{\phi}^{XY}_{LM} [\bar{\phi}^{X'Y'}_{L'M'}]^* \rangle_G = \bar{N}^{(0)}_L(XY, X'Y') \delta_{LL'} \delta_{MM'}$ where

$$\bar{N}^{(0)}_L(XY, X'Y') = \frac{1}{4(2L+1)} \sum_{l_1 l_2} [\mathcal{W}^{XY}_{l_1 l_2 L}]^* F^X_{l_1} F^Y_{l_2} \left(\mathcal{W}^{X'Y'}_{l_1 l_2 L} F^{X'}_{l_1} F^{Y'}_{l_2} C^{XX'}_{l_1,\mathrm{tot}} C^{YY'}_{l_2,\mathrm{tot}} + \mathcal{W}^{Y'X'}_{l_1 l_2 L} F^{Y'}_{l_1} F^{X'}_{l_2} C^{XY'}_{l_1,\mathrm{tot}} C^{YX'}_{l_2,\mathrm{tot}} \right) . \quad \text{(A.10)}$$

The minimum-variance combination of (a subset of) the individual quadratic estimators is approximately $\hat{\phi}^{MV}_{LM} = \sum_{XY} \bar{\phi}^{XY}_{LM} / \sum_{XY} \mathcal{R}^{XY}_L$, and has reconstruction noise power

$$N^{(0)}_L(MV) = \frac{1}{\left(\sum_{XY} \mathcal{R}^{XY}_L\right)^2} \sum_{XY} \sum_{X'Y'} \bar{N}^{(0)}_L(XY, X'Y') . \quad \text{(A.11)}$$

Acknowledgments

AC and RA acknowledge support from the UK Science and Technology Facilities Council (grant number ST/N000927/1) as does AL (grant number ST/L000652/1). AL and JC acknowledge support from the European Research Council under the European Union's Seventh Framework Programme (FP/2007-2013) / ERC Grant Agreement No. [616170]. J.G.N. acknowledges financial support from the Spanish MINECO for a 'Ramon y Cajal' Fellowship (RYC-2013-13256) and the I+D 2015 project AYA2015-65887-P (MINECO/FEDER)." CJM is supported by an FCT Research Professorship, contract reference IF/00064/2012, funded by FCT/MCTES (Portugal) and POPH/FSE (EC). Some of the results in this paper have been derived using the `HEALPix` package [128].

References

[1] A. Lewis and A. Challinor, *Weak gravitational lensing of the CMB*, *Phys. Rept.* **429** (2006) 1–65, [astro-ph/0601594].

[2] W. Hu, *Dark synergy: Gravitational lensing and the CMB*, *Phys. Rev.* **D65** (2002) 023003, [astro-ph/0108090].

[3] B. D. Sherwin et al., *Evidence for Dark Energy from the Cosmic Microwave Background Alone Using the Atacama Cosmology Telescope Lensing Measurements*, *Phys. Rev. Lett.* **107** (2011) 021302, [1105.0419].

[4] Planck Collaboration, *Planck 2015 results. XV. Gravitational lensing*, *Astron. Astrophys.* **594** (2016) A15, [1502.01591].

[5] A. Vallinotto, *Using Cosmic Microwave Background Lensing to Constrain the Multiplicative Bias of Cosmic Shear*, *Astrophys. J.* **759** (2012) 32, [1110.5339].

[6] M. Kesden, A. Cooray and M. Kamionkowski, *Separation of gravitational wave and cosmic shear contributions to cosmic microwave background polarization*, *Phys. Rev. Lett.* **89** (2002) 011304, [astro-ph/0202434].

[7] L. Knox and Y.-S. Song, *A Limit on the detectability of the energy scale of inflation*, *Phys. Rev. Lett.* **89** (2002) 011303, [astro-ph/0202286].

[8] U. Seljak and C. M. Hirata, *Gravitational lensing as a contaminant of the gravity wave signal in CMB*, *Phys. Rev.* **D69** (2004) 043005, [astro-ph/0310163].

[9] K. M. Smith, O. Zahn and O. Dore, *Detection of Gravitational Lensing in the Cosmic Microwave Background*, *Phys. Rev.* **D76** (2007) 043510, [0705.3980].

[10] S. Das et al., *Detection of the Power Spectrum of Cosmic Microwave Background Lensing by the Atacama Cosmology Telescope*, *Phys. Rev. Lett.* **107** (2011) 021301, [1103.2124].

[11] POLARBEAR Collaboration, *Measurement of the Cosmic Microwave Background Polarization Lensing Power Spectrum with the POLARBEAR experiment*, *Phys. Rev. Lett.* **113** (2014) 021301, [1312.6646].

[12] K. T. Story et al., *A Measurement of the Cosmic Microwave Background Gravitational Lensing Potential from 100 Square Degrees of SPTpol Data*, *Astrophys. J.* **810** (2015) 50, [1412.4760].

[13] B. D. Sherwin et al., *Two-season Atacama Cosmology Telescope polarimeter lensing power spectrum*, *Phys. Rev.* **D95** (2017) 123529, [1611.09753].

[14] BICEP2/Keck Array Collaboration, *BICEP2 / Keck Array VIII: Measurement of gravitational lensing from large-scale B-mode polarization*, *Astrophys. J.* **833** (2016) 228, [1606.01968].

[15] Y. Omori et al., *A 2500 square-degree CMB lensing map from combined South Pole Telescope and Planck data*, 1705.00743.

[16] Planck Collaboration, *Planck 2013 results. XVI. Cosmological parameters*, *Astron. Astrophys.* **571** (2014) A16, [1303.5076].

[17] J. Delabrouille et al., *Exploring Cosmic Origins with CORE: Survey requirements and mission design*, 1706.04516.

[18] F. Finelli et al., *Exploring Cosmic Origins with CORE: Inflation*, 1612.08270.

[19] E. Di Valentino et al., *Exploring Cosmic Origins with CORE: Cosmological Parameters*, 1612.00021.

[20] J.-B. Melin et al., *Exploring Cosmic Origins with CORE: Cluster Science*, 1703.10456.

[21] R. Allison, P. Caucal, E. Calabrese, J. Dunkley and T. Louis, *Towards a cosmological neutrino mass detection*, *Phys. Rev.* **D92** (2015) 123535, [1509.07471].

[22] D. Hanson, A. Challinor and A. Lewis, *Weak lensing of the CMB*, *General Relativity and Gravitation* **42** (2010) 2197–2218, [0911.0612].

[23] Planck Collaboration, *Planck 2015 results. XIII. Cosmological parameters*, *Astron. Astrophys.* **594** (2016) A13, [1502.01589].

[24] M. Zaldarriaga and U. Seljak, *Gravitational lensing effect on cosmic microwave background polarization*, *Phys. Rev.* **D58** (1998) 023003, [astro-ph/9803150].

[25] M. Zaldarriaga, *Lensing of the CMB: Non-Gaussian aspects*, *Phys. Rev.* **D62** (2000) 063510, [astro-ph/9910498].

[26] W. Hu, *Angular trispectrum of the CMB*, *Phys. Rev.* **D64** (2001) 083005, [astro-ph/0105117].

[27] W. Hu, *Mapping the dark matter through the CMB damping tail*, *Astrophys. J.* **557** (2001) L79–L83, [astro-ph/0105424].

[28] T. Okamoto and W. Hu, *CMB lensing reconstruction on the full sky*, *Phys. Rev.* **D67** (2003) 083002, [astro-ph/0301031].

[29] A. Cooray and M. Kesden, *Weak lensing of the CMB: Extraction of lensing information from the trispectrum*, *New Astron.* **8** (2003) 231–253, [astro-ph/0204068].

[30] D. Hanson, A. Challinor, G. Efstathiou and P. Bielewicz, *CMB temperature lensing power reconstruction*, *Phys. Rev.* **D83** (2011) 043005, [1008.4403].

[31] M. Bucher, C. S. Carvalho, K. Moodley and M. Remazeilles, *CMB lensing reconstruction in real space*, *Phys. Rev.* **D85** (2012) 043016, [1004.3285].

[32] W. Hu and T. Okamoto, *Mass reconstruction with CMB polarization*, *Astrophys. J.* **574** (2002) 566–574, [astro-ph/0111606].

[33] CMB-S4 Collaboration, *CMB-S4 Science Book, First Edition*, 1610.02743.

[34] C. M. Hirata and U. Seljak, *Analyzing weak lensing of the cosmic microwave background using the likelihood function*, *Phys. Rev.* **D67** (2003) 043001, [astro-ph/0209489].

[35] C. M. Hirata and U. Seljak, *Reconstruction of lensing from the cosmic microwave background polarization*, *Phys. Rev.* **D68** (2003) 083002, [astro-ph/0306354].

[36] E. Anderes, B. Wandelt and G. Lavaux, *Bayesian inference of CMB gravitational lensing*, *Astrophys. J.* **808** (2015) 152, [1412.4079].

[37] J. Carron and A. Lewis, *Maximum a posteriori CMB lensing reconstruction*, 1704.08230.

[38] A. van Engelen, S. Bhattacharya, N. Sehgal, G. P. Holder, O. Zahn and D. Nagai, *CMB Lensing Power Spectrum Biases from Galaxies and Clusters using High-angular Resolution Temperature Maps*, *Astrophys. J.* **786** (2014) 13, [1310.7023].

[39] K. M. Smith et al., *CMBPol Mission Concept Study: Gravitational Lensing*, *AIP Conf. Proc.* **1141** (2009) 121, [0811.3916].

[40] K. N. Abazajian et al., *Light Sterile Neutrinos: A White Paper*, 1204.5379.

[41] Particle Data Group collaboration, C. Patrignani et al., *Review of Particle Physics*, *Chin. Phys.* **C40** (2016) 100001.

[42] S. Dell'Oro, S. Marcocci and F. Vissani, *New expectations and uncertainties on neutrinoless double beta decay*, *Phys. Rev.* **D90** (2014) 033005, [1404.2616].

[43] S. Alam et al., *The clustering of galaxies in the completed SDSS-III Baryon Oscillation Spectroscopic Survey: cosmological analysis of the DR12 galaxy sample*, 1607.03155.

[44] J. Lesgourgues and S. Pastor, *Massive neutrinos and cosmology*, *Phys. Rept.* **429** (2006) 307–379, [astro-ph/0603494].

[45] Z. Pan, L. Knox and M. White, *Dependence of the Cosmic Microwave Background Lensing Power Spectrum on the Matter Density*, *Mon. Not. Roy. Astron. Soc.* **445** (2014) 2941–2945, [1406.5459].

[46] Z. Pan and L. Knox, *Constraints on neutrino mass from Cosmic Microwave Background and Large Scale Structure*, *Mon. Not. Roy. Astron. Soc.* **454** (2015) 3200–3206, [1506.07493].

[47] A. Font-Ribera, P. McDonald, N. Mostek, B. A. Reid, H.-J. Seo and A. Slosar, *DESI and other dark energy experiments in the era of neutrino mass measurements*, *JCAP* **1405** (2014) 023, [1308.4164].

[48] T. Essinger-Hileman et al., *CLASS: the cosmology large angular scale surveyor*, in *Millimeter, Submillimeter, and Far-Infrared Detectors and Instrumentation for Astronomy VII*, vol. 9153 of *Proc. SPIE*, p. 91531I, 2014. 1408.4788. DOI.

[49] Planck Collaboration, *Planck intermediate results. XLVI. Reduction of large-scale systematic effects in HFI polarization maps and estimation of the reionization optical depth*, *Astron. Astrophys.* **596** (2016) A107, [1605.02985].

[50] S. Bashinsky and U. Seljak, *Neutrino perturbations in CMB anisotropy and matter clustering*, *Phys. Rev.* **D69** (2004) 083002, [astro-ph/0310198].

[51] S. Galli et al., *CMB polarization can constrain cosmology better than CMB temperature*, *Phys. Rev.* **D90** (2014) 063504, [1403.5271].

[52] M. R. Becker et al., *Cosmic shear measurements with Dark Energy Survey Science Verification data*, *Phys. Rev.* **D94** (2016) 022002, [1507.05598].

[53] H. Hildebrandt et al., *KiDS-450: Cosmological parameter constraints from tomographic weak gravitational lensing*, *Mon. Not. Roy. Astron. Soc.* **465** (2017) 1454, [1606.05338].

[54] LSST Dark Energy Science Collaboration, *Large Synoptic Survey Telescope: Dark Energy Science Collaboration*, *ArXiv e-prints* (2012) , [1211.0310].

[55] L. Amendola et al., *Cosmology and Fundamental Physics with the Euclid Satellite*, *Living Reviews in Relativity* **16** (2013) 6, [1206.1225].

[56] B. Joachimi et al., *Galaxy alignments: An overview*, *Space Sci. Rev.* **193** (2015) 1–65, [1504.05456].

[57] S. Das, J. Errard and D. Spergel, *Can CMB Lensing Help Cosmic Shear Surveys?*, 1311.2338.

[58] E. Schaan, E. Krause, T. Eifler, O. Doré, H. Miyatake, J. Rhodes et al., *Looking through the same lens: Shear calibration for LSST, Euclid, and WFIRST with stage 4 CMB lensing*, *Phys. Rev.* **D95** (2017) 123512, [1607.01761].

[59] A. Hall and A. Taylor, *Intrinsic alignments in the cross-correlation of cosmic shear and CMB weak lensing*, *Mon. Not. Roy. Astron. Soc.* **443** (2014) L119, [1401.6018].

[60] M. Troxel and M. Ishak, *Cross-correlation between cosmic microwave background lensing and galaxy intrinsic alignment as a contaminant to gravitational lensing cross-correlated probes of the universe*, *Phys. Rev.* **D89** (2014) 063528, [1401.7051].

[61] P. Larsen and A. Challinor, *Intrinsic alignment contamination to CMB lensing-galaxy weak lensing correlations from tidal torquing*, *Mon. Not. Roy. Astron. Soc.* **461** (2016) 4343–4352, [1510.02617].

[62] N. Hand et al., *First Measurement of the Cross-Correlation of CMB Lensing and Galaxy Lensing*, *Phys. Rev.* **D91** (2015) 062001, [1311.6200].

[63] J. Liu and J. C. Hill, *Cross-correlation of Planck CMB Lensing and CFHTLenS Galaxy Weak Lensing Maps*, *Phys. Rev.* **D92** (2015) 063517, [1504.05598].

[64] D. Kirk et al., *Cross-correlation of gravitational lensing from DES Science Verification data with SPT and Planck lensing*, *Mon. Not. Roy. Astron. Soc.* **459** (2016) 21–34, [1512.04535].

[65] S. Singh, R. Mandelbaum and J. R. Brownstein, *Cross-correlating Planck CMB lensing with SDSS: Lensing-lensing and galaxy-lensing cross-correlations*, *Mon. Not. Roy. Astron. Soc.* **464** (2017) 2120–2138, [1606.08841].

[66] J. Harnois-Déraps et al., *KiDS-450: Tomographic Cross-Correlation of Galaxy Shear with Planck Lensing*, 1703.03383.

[67] T. D. Kitching, A. F. Heavens and S. Das, *3D Weak Gravitational Lensing of the CMB and Galaxies*, *Mon. Not. Roy. Astron. Soc.* **449** (2015) 2205–2214, [1408.7052].

[68] T. Giannantonio et al., *CMB lensing tomography with the DES Science Verification galaxies*, *Mon. Not. Roy. Astron. Soc.* **456** (2016) 3213–3244, [1507.05551].

[69] F. Bianchini et al., *Toward a tomographic analysis of the cross-correlation between Planck CMB lensing and H-ATLAS galaxies*, *Astrophys. J.* **825** (2016) 24, [1511.05116].

[70] C. M. Hirata, S. Ho, N. Padmanabhan, U. Seljak and N. A. Bahcall, *Correlation of CMB with large-scale structure: II. Weak lensing*, *Phys. Rev.* **D78** (2008) 043520, [0801.0644].

[71] C. Feng, G. Aslanyan, A. V. Manohar, B. Keating, H. P. Paar and O. Zahn, *Measuring gravitational lensing of the cosmic microwave background using cross correlation with large scale structure*, *Phys. Rev.* **D86** (2012) 063519, [1207.3326].

[72] L. E. Bleem et al., *A Measurement of the Correlation of Galaxy Surveys with CMB Lensing Convergence Maps from the South Pole Telescope*, *Astrophys. J. Lett.* **753** (2012) L9, [1203.4808].

[73] B. D. Sherwin et al., *The Atacama Cosmology Telescope: Cross-correlation of cosmic microwave background lensing and quasars*, *Phys. Rev.* **D86** (2012) 083006, [1207.4543].

[74] F. Bianchini et al., *Cross-correlation between the CMB lensing potential measured by Planck and high-z sub-mm galaxies detected by the Herschel-ATLAS survey*, *Astrophys. J.* **802** (2015) 64, [1410.4502].

[75] A. Kuntz, *Cross-correlation of CFHTLenS galaxy catalogue and Planck CMB lensing using the halo model prescription*, *Astron. Astrophys.* **584** (2015) A53, [1510.00398].

[76] Y. Omori and G. Holder, *Cross-Correlation of CFHTLenS Galaxy Number Density and Planck CMB Lensing*, 1502.03405.

[77] Y.-S. Song, A. Cooray, L. Knox and M. Zaldarriaga, *The Far-infrared background correlation with CMB lensing*, *Astrophys. J.* **590** (2003) 664–672, [astro-ph/0209001].

[78] Planck Collaboration, *Planck 2013 results. XVIII. Gravitational lensing-infrared background correlation*, *Astron. Astrophys.* **571** (2014) A18, [1303.5078].

[79] G. P. Holder et al., *A Cosmic Microwave Background Lensing Mass Map and Its Correlation with the Cosmic Infrared Background*, *Astrophys. J.* **771** (2013) L16, [1303.5048].

[80] A. van Engelen et al., *The Atacama Cosmology Telescope: Lensing of CMB Temperature and Polarization Derived from Cosmic Infrared Background Cross-Correlation*, *Astrophys. J.* **808** (2015) 7, [1412.0626].

[81] POLARBEAR Collaboration, *Evidence for Gravitational Lensing of the Cosmic Microwave Background Polarization from Cross-correlation with the Cosmic Infrared Background*, *Phys. Rev. Lett.* **112** (2014) 131302, [1312.6645].

[82] R. A. Sunyaev and Ya. B. Zeldovich, *Microwave background radiation as a probe of the contemporary structure and history of the universe*, *Ann. Rev. Astron. Astrophys.* **18** (1980) 537–560.

[83] J. C. Hill and D. N. Spergel, *Detection of thermal SZ-CMB lensing cross-correlation in Planck nominal mission data*, *JCAP* **1402** (2014) 030, [1312.4525].

[84] Planck Collaboration, *Planck 2015 results. XXII. A map of the thermal Sunyaev-Zeldovich effect*, *Astron. Astrophys.* **594** (2016) A22, [1502.01596].

[85] J. E. Geach et al., *A Direct Measurement of the Linear Bias of Mid-infrared-selected Quasars at $z \approx 1$ Using Cosmic Microwave Background Lensing*, *Astrophys. J.* **776** (2013) L41, [1307.1706].

[86] M. Kamionkowski, A. Kosowsky and A. Stebbins, *A Probe of primordial gravity waves and vorticity*, *Phys. Rev. Lett.* **78** (1997) 2058–2061, [astro-ph/9609132].

[87] U. Seljak and M. Zaldarriaga, *Signature of gravity waves in polarization of the microwave background*, *Phys. Rev. Lett.* **78** (1997) 2054–2057, [astro-ph/9609169].

[88] BICEP2/Keck Array Collaboration, *Improved Constraints on Cosmology and Foregrounds from BICEP2 and Keck Array Cosmic Microwave Background Data with Inclusion of 95 GHz Band*, *Phys. Rev. Lett.* **116** (2016) 031302, [1510.09217].

[89] A. Challinor and A. Lewis, *Lensed CMB power spectra from all-sky correlation functions*, *Phys. Rev.* **D71** (2005) 103010, [astro-ph/0502425].

[90] A. A. Starobinsky, *A New Type of Isotropic Cosmological Models Without Singularity*, *Phys. Lett.* **B91** (1980) 99–102.

[91] J. Carron, A. Lewis and A. Challinor, *Internal delensing of Planck CMB temperature and polarization*, *JCAP* **1705** (2017) 035, [1701.01712].

[92] G. Simard, D. Hanson and G. Holder, *Prospects for Delensing the Cosmic Microwave Background for Studying Inflation*, *Astrophys. J.* **807** (2015) 166, [1410.0691].

[93] B. D. Sherwin and M. Schmittfull, *Delensing the CMB with the Cosmic Infrared Background*, *Phys. Rev.* **D92** (2015) 043005, [1502.05356].

[94] P. Larsen, A. Challinor, B. D. Sherwin and D. Mak, *Demonstration of cosmic microwave background delensing using the cosmic infrared background*, *Phys. Rev. Lett.* **117** (2016) 151102, [1607.05733].

[95] A. Manzotti et al., *CMB Polarization B-mode Delensing with SPTpol and Herschel*, 1701.04396.

[96] B. Yu, J. C. Hill and B. D. Sherwin, *Multi-tracer CMB delensing maps from Planck and WISE data*, 1705.02332.

[97] J. Errard, S. M. Feeney, H. V. Peiris and A. H. Jaffe, *Robust forecasts on fundamental physics from the foreground-obscured, gravitationally-lensed CMB polarization*, *JCAP* **1603** (2016) 052, [1509.06770].

[98] Planck Collaboration, *Planck 2015 results. XXIV. Cosmology from Sunyaev-Zeldovich cluster counts*, *Astron. Astrophys.* **594** (2016) A24, [1502.01597].

[99] M. Hasselfield et al., *The Atacama Cosmology Telescope: Sunyaev-Zel'dovich selected galaxyclusters at 148 GHz from three seasons of data*, *JCAP* **1307** (2013) 008, [1301.0816].

[100] L. E. Bleem et al., *Galaxy Clusters Discovered via the Sunyaev-Zel'dovich Effect in the 2500-square-degree SPT-SZ survey*, *Astrophys. J. Suppl.* **216** (2015) 27, [1409.0850].

[101] D. Nagai, A. V. Kravtsov and A. Vikhlinin, *Effects of Galaxy Formation on Thermodynamics of the Intracluster Medium*, *Astrophys. J.* **668** (2007) 1–14, [astro-ph/0703661].

[102] R. Piffaretti and R. Valdarnini, *Total mass biases in X-ray galaxy clusters*, *Astron. Astrophys.* **491** (2008) 71, [0808.1111].

[103] M. Meneghetti, E. Rasia, J. Merten, F. Bellagamba, S. Ettori, P. Mazzotta et al., *Weighing simulated galaxy clusters using lensing and X-ray*, *Astron. Astrophys.* **514** (2010) A93, [0912.1343].

[104] N. Battaglia et al., *Weak-Lensing Mass Calibration of the Atacama Cosmology Telescope Equatorial Sunyaev-Zeldovich Cluster Sample with the Canada-France-Hawaii Telescope Stripe 82 Survey*, *JCAP* **1608** (2016) 013, [1509.08930].

[105] U. Seljak and M. Zaldarriaga, *Lensing induced cluster signatures in cosmic microwave background*, *Astrophys. J.* **538** (2000) 57–64, [astro-ph/9907254].

[106] C. Vale, A. Amblard and M. J. White, *Cluster lensing of the CMB*, *New Astron.* **10** (2004) 1–15, [astro-ph/0402004].

[107] G. P. Holder and A. Kosowsky, *Gravitational lensing of the microwave background by galaxy clusters*, *Astrophys. J.* **616** (2004) 8–15, [astro-ph/0401519].

[108] M. Maturi, M. Bartelmann, M. Meneghetti and L. Moscardini, *Gravitational lensing of the CMB by galaxy clusters*, *Astron. Astrophys.* **436** (2005) 37–46, [astro-ph/0408064].

[109] W. Hu, S. DeDeo and C. Vale, *Cluster Mass Estimators from CMB Temperature and Polarization Lensing*, *New J. Phys.* **9** (2007) 441, [astro-ph/0701276].

[110] J. Yoo and M. Zaldarriaga, *Improved estimation of cluster mass profiles from the cosmic microwave background*, *Phys. Rev.* **D78** (2008) 083002, [0805.2155].

[111] J. F. Navarro, C. S. Frenk and S. D. M. White, *A Universal density profile from hierarchical clustering*, *Astrophys. J.* **490** (1997) 493–508, [astro-ph/9611107].

[112] J.-B. Melin and J. G. Bartlett, *Measuring cluster masses with CMB lensing: a statistical approach*, *Astron. Astrophys.* **578** (2015) A21, [1408.5633].

[113] A. Lewis and L. King, *Cluster masses from CMB and galaxy weak lensing*, *Phys. Rev.* **D73** (2006) 063006, [astro-ph/0512104].

[114] E. J. Baxter et al., *A Measurement of Gravitational Lensing of the Cosmic Microwave Background by Galaxy Clusters Using Data from the South Pole Telescope*, *Astrophys. J.* **806** (2015) 247, [1412.7521].

[115] Planck Collaboration, *Planck intermediate results. XXX. The angular power spectrum of polarized dust emission at intermediate and high Galactic latitudes*, *Astron. Astrophys.* **586** (2016) A133, [1409.5738].

[116] B. Array and Planck Collaborations, *Joint Analysis of BICEP2/Keck Array and Planck Data*, *Phys. Rev. Lett.* **114** (2015) 101301, [1502.00612].

[117] Y. Fantaye, C. Baccigalupi, S. M. Leach and A. P. S. Yadav, *CMB lensing reconstruction in the presence of diffuse polarized foregrounds*, *JCAP* **12** (2012) 017, [1207.0508].

[118] R. Pearson, B. Sherwin and A. Lewis, *CMB lensing reconstruction using cut sky polarization maps and pure-B modes*, *Phys. Rev.* **D90** (2014) 023539, [1403.3911].

[119] W. Stein, *Infrared Radiation from Interstellar Grains*, *Astrophys. J.* **144** (1966) 318.

[120] H. M. Lee and B. T. Draine, *Infrared extinction and polarization due to partially aligned spheroidal grains - Models for the dust toward the BN object*, *Astrophys. J.* **290** (1985) 211–228.

[121] Planck Collaboration, *Planck intermediate results. XXI. Comparison of polarized thermal emission from Galactic dust at 353 GHz with interstellar polarization in the visible*, *Astron. Astrophys.* **576** (2015) A106, [1405.0873].

[122] F. Vansyngel, F. Boulanger, T. Ghosh, B. D. Wandelt, J. Aumont, A. Bracco et al., *Statistical simulations of the dust foreground to CMB polarization*, 1611.02577.

[123] T. Namikawa, D. Hanson and R. Takahashi, *Bias-hardened CMB lensing*, *Mon. Not. Roy. Astron. Soc.* **431** (2013) 609–620, [1209.0091].

[124] T. Ghosh et al., *Modelling and simulation of large-scale polarized dust emission over the southern Galactic cap using the GASS HI data*, *Astron. Astrophys.* **601** (2017) A71, [1611.02418].

[125] Planck Collaboration, *Planck 2015 results. XII. Full Focal Plane simulations*, *Astron. Astrophys.* **594** (2016) A12, [1509.06348].

[126] S. E. Clark, J. C. Hill, J. E. G. Peek, M. E. Putman and B. L. Babler, *Neutral Hydrogen Structures Trace Dust Polarization Angle: Implications for Cosmic Microwave Background Foregrounds*, *Phys. Rev. Lett.* **115** (2015) 241302, [1508.07005].

[127] M. Remazeilles et al., *Exploring Cosmic Origins with CORE: B-mode Component Separation*, 1704.04501.

[128] K. M. Gorski, E. Hivon, A. J. Banday, B. D. Wandelt, F. K. Hansen, M. Reinecke et al., *HEALPix - A Framework for high resolution discretization, and fast analysis of data distributed on the sphere*, *Astrophys. J.* **622** (2005) 759–771, [astro-ph/0409513].